CIRP Annals - Manufacturing Technology 74 (2025) 1019–1045

Contents lists available at ScienceDirect

CIRP Annals - Manufacturing Technology

journal homepage: https://www.editorialmanager.com/CIRP/default.aspx

Surface finishing by shape-adaptive processes

Jiwang Yan (1)[a,*], Brigid Mullany (1)[b], Anthony Beaucamp (2)[a], Daniel Meyer (2)[c], Naohiko Sugita (1)[d]

[a] Faculty of Science and Technology, Keio University, Yokohama, Japan
[b] Department of Mechanical Engineering & Engineering Science, University of North Carolina at Charlotte, Charlotte, USA
[c] University of Bremen, Faculty of Production Engineering, Leibniz Institute for Materials Engineering IWT, Bremen, Germany
[d] Department of Mechanical Engineering, Graduate School of Engineering, University of Tokyo, Tokyo, Japan

ARTICLE INFO

Article history:
Available online 6 June 2025

Keywords:
Surface
Finishing
Geometry
Shape-adaptive process

ABSTRACT

Complex surfaces are increasingly used in optics, biomedical devices, and aerospace industries. Additive manufacturing and five-axis milling can produce complex shapes, but additional finishing processes are needed to meet the surface quality demands. This keynote paper reviews shape-adaptive finishing processes that enable uniform surface quality improvement without altering the shape. Key factors affecting shape adaptability, processing efficiency, and material applicability are analyzed and optimal process selection strategies for finishing complex surfaces are discussed. Future possibilities and research topics in this area, including process modeling/simulation, digital twin, surface/subsurface metrology, functionality evaluation, and applications of advanced robotics and artificial intelligence, are outlined.

1. Introduction

The expanding design space realized by improved modelling, design, and fabrication capabilities has resulted in a great variety of component geometries being produced to meet a wide range of increasingly stringent functionality requirements. Especially in recent years components with complex three-dimensional shapes have become more prevalent in various fields. For example, free-form optics used in virtual reality (VR) and augmented reality (AR) systems [67], artificial joints and dental implants used in biomedical field [90], precision molding dies used in plastic/metal forming [243], and turbomachinery components used in electrical generator, vessels, and airplane jet engines [119]. Generally, these components are required to have both high form accuracy and surface quality to meet the requirements of functionality. For example, the form accuracy and surface roughness of freeform optics are required to be in the levels of 0.1 μm *Sz* (peak to valley) and 1 nm *Sa* (average roughness), respectively [67], and these values become smaller for shorter wavelength applications such as UV optics. Sometimes, high surface quality is required mainly for aesthetics/cosmetics purposes to achieve visual/haptic comfort, and in turn, adding value to products, such as artworks, ornaments, accessories, and portable/wearable devices.

A complex shape can be fabricated via additive, subtractive manufacturing processes, or forming methods. In recent years, numerous methods of additive manufacturing have been developed for creating complex shapes of various materials [206]. However, due to the powder particle size, melting parameters, layer thickness and the orientation/slope of surfaces, the additive-manufactured part surfaces are usually very rough with *Ra* ranging in the level of 1~10 μm, which is far rougher than being usable as final products [70]. Similarly, in subtractive manufacturing methods, such as multi-axis milling, tool feed marks and burr formation may result in rough surfaces [126]. As functionality requirements increase, whether due to more challenging operating conditions or the desire for enhanced longevity, achieving the texture and quality of the component's surface and subsurface through the process used to create its overall geometric form becomes unlikely. In such cases, additional processes, possibly employing different physical mechanisms than those used for form generation, are necessary to finish the surfaces and meet the required specifications across relevant length scales in terms of form accuracy and surface quality.

Extensive research has been conducted on surface finishing of semiconductor wafers where a uniform pressure is applied to a flat workpiece [65]. A main challenge in finishing complex surfaces is ensuring that the material removal/deformation rate remains consistent irrespective of the surface's geometric form. The surface finishing system must enable adaptive control of the dominating process parameters, i.e. applied load, relative velocity profiles, to accommodate the workpiece shape. Finishing complex surfaces has been often performed manually by skilled workers, but there is a great drive to replace them with deterministic, automated, and controlled processes. The shape adaptability of the process may be achieved by machine movement, tool compliance, or a combination of both. A shape-adaptive process reduces surface roughness uniformly while keeping the desired workpiece shape. In addition, to make the process cost effective, surface finishing must be performed efficiently. This means the process must meet the requirements of shape adaptability, surface quality and production efficiency simultaneously.

* Corresponding author.
E-mail address: yan@mech.keio.ac.jp (J. Yan).

https://doi.org/10.1016/j.cirp.2025.04.084

In recent decades, several surface finishing technologies have been developed which can be used for finishing complex surfaces. These processes are based on multidisciplinary mechanisms, such as mechanical, thermal, chemical, physical modification of surfaces. Various types of tools have been used for shape-adaptive surface finishing, such as deformable solid tools, fluid jet tools, powder-based tools, high energy beam tools, and so on. Surface finishing of various workpiece materials such as pure metals, alloys, glass, ceramics, polymers, and composites, has been investigated. These new finishing processes have enabled a bigger design space and added value for complex geometries.

Within the framework of the International Academy for Production Engineering (CIRP), several keynote papers have been published on the theme of complex surfaces manufacturing, such as freeform surfaces [67] and structured surfaces [44]. While considerable efforts have been invested in the shape design and creation [190], metrology of complex surfaces [76], as well as modelling of surface generation at the micro-nano scales [237], less review papers can be found which focus on the finishing processes for such surfaces. In this context, a review of the shape-adaptive surface finishing technologies for complex surfaces is considered a timely contribution to the community of manufacturing.

This paper consequently reviews the advances in the research and development (R&D) of shape-adaptive processes for complex surface finishing and identifies the challenges in finding optimal finishing processes compatible with the process chains used to generate the form and to achieve the final desired specifications. Section 2 introduces the relevant terminology and classification of the processes discussed in this paper in terms of their surface modification mechanisms and tooling mechanisms. Sections 3 to 6 provide comprehensive reviews of typical methods for shape-adaptive surface finishing, including mechanical (with/without material removal), chemical, and physical methods, respectively. Section 7 presents a comparative analysis of the shape adaptability, material applicability, processing efficiency, and achievable surface quality for the methods described in Sections 3 to 6. Based on the review and analysis of the state of the art of complex-shape surface finishing, Section 8 discusses future possibilities and promising research topics in this area. Finally, Section 9 summarizes the main conclusions.

2. Definitions

2.1. Geometries requiring shape-adaptive processes

The design requirements of a surface that necessitate the application of shape-adaptive finishing processes typically include some or all of the following: continuous surfaces with varying radii of curvature, discontinuous surfaces with features such as facets or steps, discrete local features on continuous surfaces, or a combination of multiple non-complex surfaces arranged in complex manner. Not included in this paper are the fabrication of multiscale structured surfaces as outlined in the 2020 CIRP keynote [44]. The creation of deterministic features of shorter length scale, and lower amplitude values on the surfaces described earlier in this section are not considered here, however the final finishing of such created features are within the scope of the paper.

2.2. Core aspects of shape-adaptive processes

Shape-adaptive processes for finishing complex surfaces are those that can accommodate local changes in surface topography, through deterministic, ideally in-process, control of the tool-workpiece interaction. In this context, 'in-process' refers to the on-machine measurement of workpiece surface carried out while the manufacturing process is taking place [76]. The tool-workpiece interaction mechanisms may be mechanical, chemical, or physical in nature, as shown in Table 1. Irrespective of the mechanism, material removal and/or material re-distribution will occur on the workpiece surface. For a tooling configuration, the tool's removal or modification rate, referred to as the tool influence function (TIF), should ideally be deterministic and controllable [110]. In all cases, it is imperative to understand the factors affecting the resulting topography (form variation and surface finish) achievable by the TIF. Whereby form variation is in the order of the tooling size, surface finish is focused on high spatial frequency surface characteristics such as root mean square roughness (Sq) or similar parameters according to ISO 25178-2 [99].

Table 1
An overview of shape-adaptive surface finishing processes

Primary mechanism	Subcategory	Processes
Mechanical with material removal	Loose Abrasive	Tool-based polishing
		Contactless processing
	Fixed Abrasive	Compliant grinding
		Belt finishing
	Kinetic Abrasive	Mass Finishing
		Sand blasting
		Fluid jet polishing
Mechanical without material removal	Peening	Shot peening
		Water jet peening
		Machine hammer peening
	Burnishing	Roller/ball burnishing
		Deep rolling
Chemical	Liquid	Solution-based polishing
	Solid	Dry electropolishing
	Plasma	Plasma-assisted polishing
Physical	Ion/electron beam	Ion beam figuring
		Electron beam irradiation
	Laser beam	Laser peening
		Laser polishing
		Laser recovery
	Electrical discharge	Electrical discharge polishing

While the actual process mechanism and tooling configuration strongly influences the high spatial frequency (roughness) finish, the surface coverage ratio (SCR) of the tool can influence both the mid (waviness), and low (form) spatial frequency components of the processed surface. The SCR is defined as the ratio of TIF's projected area to the workpiece surface area, see equation 1:

$$SCR = TIF_{\text{projected area}}/Workpiece_{\text{surface area}} \quad (1)$$

Typically the shape and magnitude of a TIF is determined by quantifying the post processing surface under the following conditions: (1) the tooling is held at a fixed location with respect to the workpiece (or vice versa), (2) there is no tooling movement beyond that inherently required for the process mechanism, (3) the duration of the processing is for a defined period of time, known as the dwell time. See Fig. 1 for sample TIFs.

In-process variation of the TIF can be achieved via any of the following: orientation of the tool with respect to the workpiece surface (as illustrated in the top row of Fig. 1), altering the process settings to influence the magnitude of the tool's material removal or surface modification rate, or by in-process alterations of the tool's shape. This highlights another shared requirement across all shape adaptive processes, that is, the orientation and location of the tool with respect to the workpiece surface is always known.

In cases where the SCR is less than 1, the tool must translate over the workpiece surface, i.e. follow a pre-defined tool path, with a given

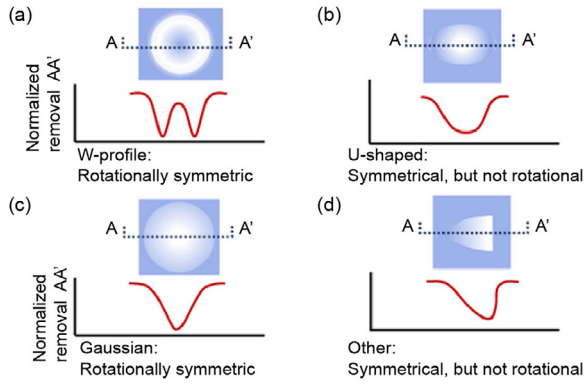

Fig. 1. Sample TIF profiles.

step over, to ensure full surface processing. The shape of the TIF combined with overlap between adjacent toolpaths results in local variations in the material removal with periodicities predictable via convolution of the TIF and the step over distance, see Fig. 2(a). These periodic surface undulations have spatial wavelengths shorter than the tooling diameter and are typically categorized as waviness or mid-spatial frequency (MSF) features on the surface. Wavelengths for such MSFs are defined by the optics industry to be 80 µm to 2.5 mm [98,198]. These MSF features, if of sufficient amplitude, will result in degradation of the system's optical performance [4,198]. Although MSF features are highly dependent on the programmed toolpath, i.e. step over between adjacent paths and the raster strategy, the latter can be chosen to reduce the nature of the MSFs on the surface by avoiding highly linear paths, changing tooling direction between subsequent passes, or programming a pseudo random path, see Fig. 2(b) [63,169,228] for examples of the latter.

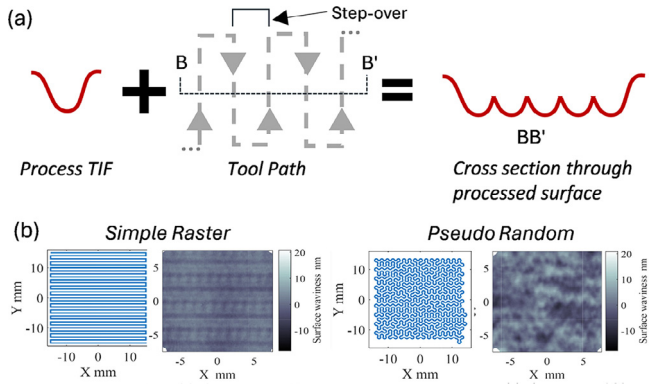

Fig. 2. (a) TIF combined with raster path can induce MSF features on the processed surface, (b) illustrates the surfaces resulting from simple raster (left) and pseudo random (right) tool paths [228].

While a TIF is typically determined when the tooling is at a specified orientation with respect to the workpiece surface, and ideally that should be maintained throughout processing, scenarios will arise where slope discontinuities and regions of high local slope gradients will occur within the TIF area, see Fig. 3. In such instances, the TIFs may vary from that nominally characterized and the potential impact of such needs to be considered with respect to the processes ability to achieve the required finish and form. This will be addressed for the processes described within Sections 3 to 6 of the paper.

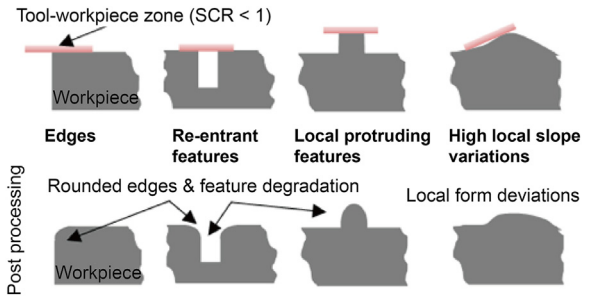

Fig. 3. Top row: examples of local geometries that pose processing challenges; Bottom row: resultant post processing form degradation.

2.3. Finishing process objectives

Finishing refers to the processing needed to achieve the required specifications across all spatial length scales, i.e. at the shorter (roughness), medium (waviness), and longer (form) length scales. While a finishing process may target a sub-set of the spatial domains, i.e. finish and/or form, it is seldom that optimal performances can be achieved without due consideration to the other spatial domains.

The final surface texture may range from stochastic to deterministic finishes, see [105] for definitions and examples. In most cases, the trend leans more towards stochastic finishes. The achievable finish, while ultimately dependent on the composition and integrity of the workpiece material, is also obviously driven by the factors controlling the process mechanisms at a local scale. For example, the size of the abrasives abrading the workpiece, compliance of the solid tool bringing the grits in contact with the workpiece, the chemical interactions between utilized fluids and the surface, laser power density, etc.

As already noted, for processes with a SCR <1, the waviness of the final surface will depend on both the shape of the TIF, its sensitivity to underlying slope variations, the chosen tool raster path, and the associated raster path's step over distance.

Considering that as the part's overall form is dependent on the longer-term stability of the TIF, i.e. over the time taken to process the entire surface, and again the sensitivity of the tool to local variations in surface slopes, a consistent dwell time over the surface is required for consistent material removal or modification. However, convolving the TIF function, and the surface height form error maps, enables the generation of a TIF dwell time map for each location on the surface. The dwell time map, which controls the tool's translation speed over the surface, indicates where the tool should move slowly (to remove more material or modify the material more intensively) and more rapidly (to remove less material or modify the material less intensively) to reduce overall form errors. While primarily utilized within the optics industry, form errors in the nanometer range are technically feasible.

3. Mechanical processes with material removal

Mechanical processes can either plastically modify surfaces via material deformation or remove the material via ductile and/or brittle modes. The removal mode and rate depend on numerous factors encompassing the workpiece material properties, processing conditions, and the tooling geometry. While this paper is more concerned about the shape adaptability of processes, key aspects of the material removal regime will be discussed in this section to provide insights on the resulting TIF shapes. Processes covered include loose abrasive processes, fixed abrasive processes, and fluid-based kinetic abrasive processes.

The TIFs encountered in this section have SCRs <0.5 (expect for mass finishing, see Section 3.3.1), so both the tool path (Fig. 2) and tooling compliance (Fig. 3) need to be considered in the context of required final specifications (form, waviness, finish). Aside from conventional material driven considerations, the choice of the finishing process also depends on both the overall shape of the surface and the severity of the local gradients. All processes in this section rely on physical contact between the abrasives and the workpiece to alter the surface, but processes requiring a tool, not a jet/stream, to engage the abrasives with the workpiece will be more sensitive to physical accessibility constraints. Concave structures, highly variable surface gradients, and surface discontinuities will be more difficult to access than convex surfaces with less surface gradients and discontinuities. While using smaller tooling diameters can improve accessibility, doing so may incur longer tool paths/processing times, wear induced changes to the TIF, leading to unpredictable form and finish variations, and the potential for difficult-to-remove short wavelength MSFs.

To understand the nature of the resulting TIFs and how they may or may not accommodate gradient variations within the TIF's projected area, the material removal mechanisms will be considered and discussed in each section. A shared characteristic, irrespective of the mechanical process deployed, is that the TIF shape and depth shows a strong correlation with the surface's principal curvatures [256].

If stable TIFs can be maintained across the workpiece surface, and given sufficient form metrology and computer control, deterministic finishing to correct form errors is achievable. In fact, the majority of the processes with SCRs<1 in this section have been developed by the optics industry to obtain sub-micrometer form errors on freeform surfaces.

3.1. Loose abrasive processes

3.1.1. Tool-based polishing

Pad-based (or tool-based) polishing has been used for finishing components for centuries. It is the quintessential loose abrasive

process whereby abrasive grits are fed together with a carrier fluid in front of the tool. They are then entrained by the tooling and the resulting relative motion and load applied by the tooling removes material to produce a low roughness surface. The tool consists of a rigid substrate connected to the articulation system. Polishing pads of varied stiffnesses are adhered to the substate. Contact with the workpiece is achieved via an applied load. The most basic equation used to characterize the material removal rate of loose abrasive processes is a variant of the Preston equation, which localizes the interaction of abrasives with the surface [222]:

$$\frac{\delta z}{\delta t}(x,y) = k_p \mu(x,y) v(x,y) \sigma(x,y) \quad (2)$$

where k_p is the material/grit type dependent Preston constant, $\mu(x,y)$ is the distribution of friction in the contact zone, $v(x,y)$ is the distribution of relative velocities in the contact zone (accounting for the sphericity and tilt of the tool), and $\sigma(x,y)$ is the pressure distribution in the contact zone resulting from the load applied on the tool. The tool offset into the surface, which compresses an elastic tool (made of rubber or silicone), induces the applied load. From this equation, it is clear that for a tool rotating about its own center, the TIF will have a W-shape profile as shown in Fig. 1(a). Direct prediction of the profile is difficult as the friction and pressure distribution in the contact zone are particularly difficult to characterize [222]. Other factors that play a role include hydrodynamic pressure [283], friction variations due to pad properties and slurry replenishment, as well as the influence of shear-stress-based removal. It is also noted here that this equation fails to predict the existence of material removal along the rotational axis of the tool (where velocity is zero) [97]. This is due to the chemical interactions between water and the workpiece surface (hydrolysis), often augmented by the use of chemically active abrasives such as silica or ceria, that results in a relative softening of the substrate surface hardness [65].

The achievable surface finish is determined by process consumables (abrasive type, slurry composition and pad type) [65]. While Evans et al. [65] and Cook [51] provided a solid foundational understanding of the role of consumables in conventional polishing, newer literature on the topic of chemical mechanical polishing (CMP) should also be considered. It encompasses details of optimal slurry composition for a broader range of materials beyond the conventional semiconductor materials for which the process was developed [128,214]. For example, an impeller blade made of stainless steel has been successfully polished. Compared with the surface before polishing, the tool marks and vibration defects were completely removed, resulting in a reduction of *Ra* from 1.66 to 0.56 μm [136].

It is important to maintain consistent load distribution as the tooling translates over the surface. Multi-axis machines are needed to maintain constant pressure distributions. Special planning software, which can compensate for fluctuations in the applied forces, is required to ensure that uniform material removal is achieved across the surface [130]. When using industrial robots, the lower stiffness and accuracy require the use of adaptive systems for controlling the load in the contact area [112,162,270], although the contact condition can be fully described by a set of concurrent partial differential equations that have a unique set of solutions [285].

While conventional polishing has an SCR above 1, in the 1970s Aspden et al. [12] combined small conventional polishing tool constructs (SCR<0.25) with numerical position control to better control the form achievable on an optical component. Using simple *x*-*y* position control and convolution dwell time calculations, they were able to correct form errors on an 80 cm optic with a 300 cm radius of curvature. In the 1990s, a more complex tool articulation system was presented by Ando et al [9] to finish freeform optical surfaces. Since then, deterministic polishing has evolved to attaching tools of smaller sizes to articulated robot arms with multiple degrees of freedom to ensure that the tooling remains normal to the workpiece surface at all stages during processing thus enabling the finishing of more complex freeform optics. Again, smaller tools can accommodate higher slope gradients, though West et al. [254] and Martin et al. [153] used a stressed lap whereby the form of the polishing tool was mechanically altered to accommodate local slope variances on the large meter-scale freeform mirrors for the Giant Magellan Telescope project. Irrespective of their sizes, conventional polishing tools used in this configuration have a W-shaped TIF profile. A TIF like that illustrated in Fig. 1(b) can be achieved by rotating a spherical tool that has its axis tilted with respect to the local normal of the freeform surface [245], see Fig. 4.

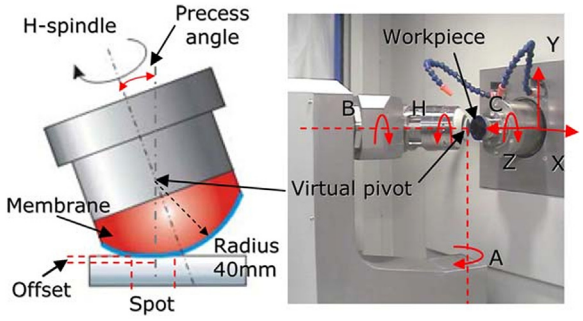

Fig. 4. Schematic of a compliant bonnet polishing tool and its implementation on a virtual pivot-based CNC machine [27].

This method has been applied to a range of compliant tools: gas-bag tools [104], bonnet tools (a reinforced membrane filled with compressed air) [245], as well as rubber/silicone and polyurethane tools [27] which can be in turn covered with conventional polishing pad materials. The direction of the tilt can be used to control the directionality of marks left on the surface by the abrasives, with continuous processing of the tool producing the best results [23]. The area of the contact region is controlled by the geometrical offset of the tool into the workpiece surface, while the load or stiffness of the tool may be controlled independently by changing the air pressure, Shore hardness of the rubber/silicone, or thickness of the rubber layer [252]. The tool radius is usually adapted to the workpiece size, with consideration given to tool accessibility with respect to the most concave curvature on the surface. The smallest radius for a rotating tool as reported in the literature is 0.4 mm [2]. Beyond that point, the rotational velocity of the tool required to achieve substantial material removal rate becomes impractical. To overcome this constraint, smaller tools can also be used on a rapidly vibrating head instead of a spindle [82,223]. In this case, the small tool radius ensures consistent removal rate under a fixed pre-load and lateral motion, regardless of the surface slope. The TIF is shaped like a groove when actuating in one direction, and like an inverted top-hat when actuating in two directions.

These tool-based loosed abrasive processes have found much application in the form correction of optical components by controlling the dwell time at each location on the tool's path. As simple raster toolpaths can induce MSFs, pseudo random paths (see Section 2.2), developed for the bonnet tools, have been deployed to avoid the generation of MSFs. While this approach can reduce the generation of highly periodic features, complete avoidance is difficult. Removal requires either the use of a low compliance tool, a fiber-based tool, or introducing a viscoelastic material instead of air inside the bonnet tool cavity [117]. If the low compliance tool (first avenue) is chosen, the pads must be sufficiently stiff so as to not contact (and hence remove material) from the lower regions of the waviness feature; however, it may induce its own form errors if not sufficiently compliant to longer scale slopes. The fiber-based tools (second avenue) can be sufficiently compliant on a longer length scale to conform to form variances, while sufficiently stiff on the local scale to only remove material from the asperities of the MSFs [208,209]. Fig. 5 illustrates the removal of surface waviness through interaction with a viscoelastic tool (third avenue).

As material removal is dependent on the load acting on the tool contacting the workpiece, all struggle to accommodate surface discontinuities that alter the pressure profiles within the TIF's projected area, see Fig. 3. Fig. 6 illustrates the higher material removal rates at

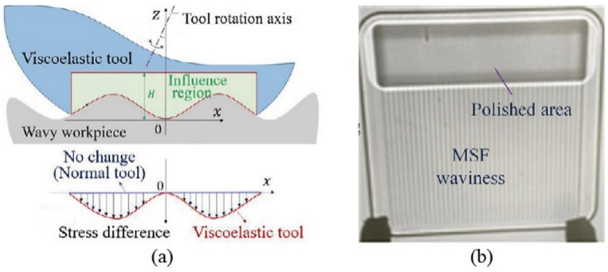

Fig. 5. (a) Interaction between viscoelastic bonnet polishing tool and surface, and (b) typical removal of mid-spatial-frequency waviness [286].

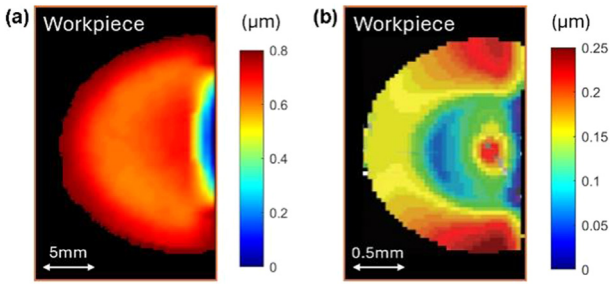

Fig. 6. TIF distortion near the edge of workpiece: (a) bonnet TIF [131], (b) fluid jet TIF [83].

the edge of the part during bonnet polishing and fluid jet polishing. However, the edge of the tool, as well as planning a progressive reduction of the spot size near the edge in the tool path, can mitigate these issues [131]. While sacrificial parts, i.e. fixtures adjacent to edges and plugs for re-entrant features to prevent tool overhang (and thus altered pressure profiles), can minimize associate edge rounding issues, maintaining the form of features smaller than the tool's TIF is not feasible with these contact-based processes, i.e. scenarios illustrated in the two right most cases illustrated in Fig. 3.

3.1.2. Contactless process

For tools not contacting the surface, the load is controlled either by the tool spinning rate (for shear-thickening fluids), or the strength of applied magnetic field (for magnetic finishing). Shear stress finishing is a recently developed abrasive based method, which was first proposed to improve the surface finishing characteristics of fluid-only based processes [133]. Based on the observation that non-Newtonian fluids, such as dense aqueous mixtures of corn starch, tend to increase their apparent viscosity when subjected to shear, the concept of dynamically jamming abrasives against the workpiece surface arose, as shown in Fig. 7. The intricacies of fluid behavior and optimization are detailed in [132,160,217,288]. It was found that the flow velocity of slurry affects shear rate in the polishing region and hence the removal rates. A modification of Preston's law has been proposed in order to characterize material removal rate (MRR) in the planar shear stress finishing process [271]:

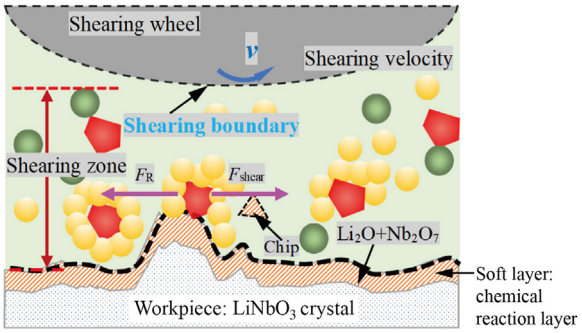

Fig. 7. Shear stress finishing mechanism: polymers or starch form hydro-clusters in the shear zone, which encapsulate the abrasives and drive them to abrade the surface [132].

$$MRR = KPv^{3-\frac{2}{n}} \quad (3)$$

where K is the lubrication coefficient, P the applied pressure on the fluid, v the relative velocity, and n is the viscosity index of the slurry (with $n = 1$ corresponding to a Newtonian fluid). At the nanoscale, abrasive interaction with the surface bears strong similarities with the float polishing process with the material removal mechanism consisting of both removal and transfer of atoms that promote a fine surface finish [31]. The approach has found application in smoothening non-trivial surface geometries: optical glass [210], gear surfaces [171], tool edges [47], V-groove micro structured surfaces [277], turbine blades [211] and prosthetic joints [170]. It has, however, not been used for form correction. The removal mechanism is entirely dependent on fluid stiffening. Since the stiffening phenomenon occurs above a critical fluid shear rate condition, small changes in the gap shape (when going across freeform surfaces) or the gap height (due to tool path deviations) can significantly alter the removal rate. This makes deterministic polishing particularly challenging.

Magnetorheological finishing (MRF) is a process that is primarily used for form correction. It utilizes an electromagnetic field to sufficiently increase the stiffness of a magnetorheological fluid containing iron carbonyl particles and polishing abrasives (ceria or diamond), so that when the stiffened fluid encounters the workpiece surface, it abrades material, see Fig. 8(a). Their uptake by the optics industry in the 90s [101] revolutionized the precision finishing of freeform surfaces. Form errors in the sub-micrometer range and nanometer scale roughness are achievable on freeform surfaces. In this application, the MRF machines are configured for the fluid to be entrained over a rotating wheel, effectively producing a renewable fine grinding wheel. While the details of the factors affecting the MRR are given by DeGroote et al. [56], the drag force as the fluid engages with the workpiece results in a TIF similar in shape to those shown in Figs. 1 (d) and 8(b). TIF lengths are typically several mm long, and depths of 0.2 mm in glass can be achieved in a few seconds. As with other wheel-based processes, the radius of curvature of the wheel carrying the fluid to the workpiece dictates the scale and geometry of the part that can be finished. The supplied smallest wheel diameter is 10 mm.

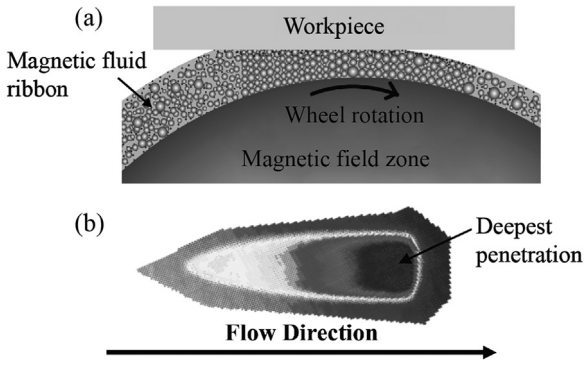

Fig. 8. (a) Schematic of MRF configuration, (b) example TIF [56].

Magnetic field assisted finishing (MAF) utilizing ferri-colloid solution mixed with abrasives and conventional magnetic poles was driven by the need to polish difficult-to-access surface, such as the internal walls of fine ceramic tubes [248]. Such a configuration was found to offer a fast and easily controllable method to finish internal surfaces down to around 0.01 μm Ra [224]. The process could be accelerated by introducing a specially prepared pole inside the tube, which is attracted to the magnetic field and increases the area of contact processing [260]. The process was later adapted to polishing complex freeform surfaces such as prosthetic knee joint [259], stents [261] and V-grooves [251], by adopting a shaft configuration that presses the magnetic particles against the workpiece. The distribution of abrasives around the tip can be inferred from the magnetic equipotential between the tip and workpiece, as shown in Fig. 9. Concentration of the magnetic field in preferential areas can be achieved by including magnetic-field shielding material (Mu-metal) in the shaft construction [16].

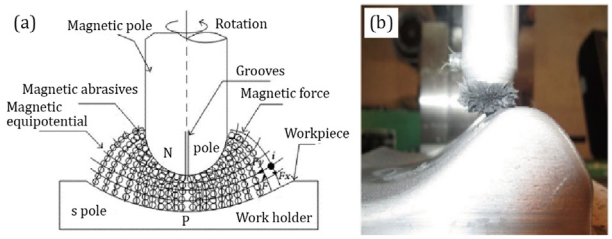

Fig. 9. Magnetic finishing tip: (a) schematic of magnetic equipotential, and (b) appearance of polishing tip [244].

Alternative setups have been proposed for specific applications. For instance, the use of a rubber sheet to separate the magnetic elements and abrasives was adopted to polish diffractive optical elements without damaging the profile edges of the optics [225]. In another deployment, counter-rotating rollers were used to produce a well channeled and high-velocity flow of magnetic abrasive compound for polishing microfluidic channels [81]. A magnetic-field-assisted mass-finishing process was also reported, in which an annular chamber filled with either bonded or loose magnetic abrasive brushes is rotated past sets of paired permanent magnets [247]. Additionally, it is possible to integrate chemically active ingredients in the polishing compound, such as free radicals that etch the surface [189]. Again, these processes are primarily concerned with smoothening the surfaces, and do not target form corrections.

3.2. Fixed abrasive processes

3.2.1. Compliant grinding processes

Generally speaking, processes with fixed abrasives offer higher abrasion rates than loose abrasives and are more likely to find application in form correction and the finishing of harder materials including special alloys and ceramics [284]. However, given the rigidity of conventional metal bonded or vitrified grinding wheels, their application in finishing complex geometries is limited by the need to match the tool radii with the surface curvatures; variances in the latter will result in excess or limited local material being removed from the workpiece. Replacing the rigid matrix material with more compliant elastic material offers more flexibility as the TIF is no longer driven by the in-feed value, but rather the applied force as determined from the axial offset into the workpiece surface. The commentary made in Section 3.1 regarding TIF shapes is applicable here. Again, it is noted that precise control of tool position and load is required in order to achieve stable material removal conditions with such processes [48,81] . For this purpose, dressing the pad with a grinding tool or cutter is a common approach [27] that allows precise motion of the contact area when using precision CNC machines.

A number of compliant tools with fixed abrasives have been developed. A typical implementation is the shape adaptive process in which rigid pellets embedded with abrasive grits are firmly attached on top of an elastic spherical body [25]. At the scale of the abrasives, high mechanical impact can be attained without inducing large thermal effects. A further advantage is the existence of a defined cutting edge, as shown in observations of the tools at different stages of machining [24], which ensures a substantial and stable material removal rate from the tool. A mixture of water and mineral oil is typically supplied as a coolant. The behavior of the abrasives in shape adaptive grinding was studied in detail by Zhu et al. [287], who showed that cutting, plowing and rubbing can occur simultaneously due to the varying pressure distribution in the contact region, as shown in Fig. 10. The possible coexistence of cracking, plastic flow and elastic behavior modes within a contact region, imply that deviations from nominal TIF pressure distributions may have impact beyond the TIF profiles; local variances in surface finishes may be induced. Shape-adaptive grinding tools have been shown to achieve nanometer scale roughness *Ra* on various metal alloys and hard ceramics, often starting from a very coarse condition such as selective laser sintering [24], metal-matrix composites [287], WC-Co coatings [78], and chemical vapor deposition [29], without the need for a pre-

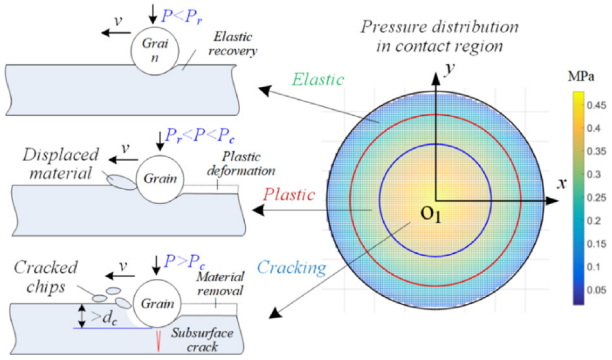

Fig. 10. Pressure distribution in a circular contact zone of a compliant spherical tool, and its effect on abrasive/workpiece interaction [283].

machining step. A further advantage of the defined cutting edges is the possibility to build predictive models of the finished surface topography [115]. When combined with a final finishing step with loose abrasives, angstrom (Å) level roughness can be achieved in applications such as X-ray mirrors [23].

Monolithic elastic grinding wheels in which the abrasives are directly embedded into rubber or polyurethane is another avenue. They have been shown to perform exceedingly well in finishing of gears, thanks to their compliance with the surface which means that the actual depth-of-cut is not a direct relation of the geometric contact condition [93], while some recent developments have attempted to hybridize loose and fixed abrasive tools. Using a dissolvable bond, a tool was developed that continuously loses fixed abrasives [262]. In another attempt, a hybrid tool combining a conventional cup grinding wheel and a shape-adaptive grinding tool demonstrated both deep axial cutting depth and significantly improved surface roughness with reduced grinding chatter [184].

3.2.2. Belt finishing processes

Belt finishing processes, where the apex of the belt contacts the workpiece, are a fundamental technique in compliant tools with fixed abrasives. They offer advantages such as smaller radii of curvature, displacement-based loading, and improved accessibility to concave geometries due to their extended length. As shown in Fig. 11, the abrasive belt grinding process primarily relies on the relative motion between abrasive grains and the workpiece under normal pressure. The complex contact deformation at the grinding interface results from the elastic properties of the belt substrate, bonding material, and rubber contact wheel [195]. Consequently, the cutting depth in abrasive belt grinding cannot be precisely controlled. Instead, the normal displacement of the grinding head (u) is commonly used to adjust the normal grinding pressure. Recent research has emphasized a deterministic approach, focusing on both form and finish to enhance the resilience of coated abrasive products used in belts. The advent of sol-gel process [118] and explosive fragmentation method [5] for production of these abrasives has proved particularly successful. Such abrasives have a micro-structure that allows them to slowly break down as they wear, instead of falling-off entirely from the abrasive sheet binder matrix. In this way, the belt can remove material for an extended time, while maintaining excellent uniformity of removal rate and surface roughness.

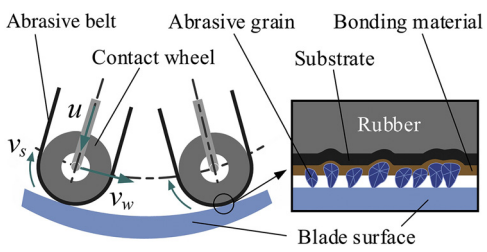

Fig. 11. Principle of belt grinding process [135].

3.3. Kinetic abrasive processes

Abrasives processes based on kinetics can be generally split into two overall categories: (1) mass finishing processes where the workpiece is either entrained in moving media, or is moved through in a deterministic matter, and (2) fluid or gas-based jets with or without abrasives that impinge the workpiece surface with a pressure significantly lower than abrasive milling jets. In each case, the abrasives or media impact and score the surface on a nanometric scale, removing minute amounts of material.

3.3.1. Mass finishing processes

Mass finishing processes enable the finishing of a wide range of geometries via the relative motion between the workpiece and the abrasive media of choice. In all cases, the SCR is larger than 1 and as such the processes are primarily for only altering the surface finishes. The processes may be fixtureless (barrel, centrifugal barrel or disk, tumbling, vibratory) or fixtured (drag or steam finishing) in nature with the latter being more suited for higher valued components where component to component impact is undesirable [18]. While these processes are simple in concept, the media-workpieces interactions, consisting of some combination of impact, sliding and rolling, are dependent on media geometry, added fluids, and system kinematics [250,258]. The latter has a significant influence on the resulting surface topography. Depending on the orientation of the workpiece surface to the dominant media flow direction, a surface may experience more rolling or sliding interactions over direct impact where rolling and impact modes will drive plastic deformation and smoothening of local surface features, while sliding is more likely to induce material removal and result in scratches. Mullany et al. [164] observed how the surface topography on opposing sides of a flat plate can vary depending on part orientation within the flow. The problem is further worsened when the surface geometry is complex or when the initial surface topography also varies with orientation, as in the case of additively manufactured components. While mass finishing processes for additively manufactured parts have been widely studied, both [18] and [70] provide good reviews, the emphasis has been placed more on average roughness reduction and how a process smoothens surfaces printed with different orientations with respect to the build direction. Papers outlining the effectiveness of different mass finishing options include [39,102,155]. For the fixtured processes (drag, stream or other variants of such) there is a need to develop modelling capabilities to optimize the orientation of the workpiece within the media flow to ensure uniform processing of all surface regions. Two different modelling approaches can be taken, neither yet fully developed. One approach is to consider the media as a continuum. Keanini et al. [114] demonstrated the validity of this approach and modelled the media using computational fluid dynamics software packages to ascertain local workpiece velocity and pressure profiles, see [164] and [73] for insights on the approach. Missing from this strategy is the integration of the actual media workpiece interactions to predict finish topography. The second approach is to use discrete element modelling (DEM) to model the media workpiece interaction [241]. In this case, the flow and contact properties of media round the workpiece can be more accurately captured, although the computation time is dramatically longer. This second approach offers great potential, albeit currently it involves high computational costs.

3.3.2. Sand blasting

For the jet-based processes, the kinetic energy of abrasive particles is the main driving factor in localized interactions with the surface. The volume V of material removed by a single particle can be simplified as follows [30]:

$$V(v_x, v_y) = k\left(\frac{1}{2}m_p v_x^2\right)\left(\frac{1}{2}m_p v_y^2\right)^{\frac{2(1-b)}{3}} \quad (4)$$

where k and b ($0.5 \leq b \leq 1$) are coefficients compounding contributions from plastic flow pressure and spring back in the material; v_x and v_y represent the tangential and normal speed, respectively; m_p is the mass of the abrasive particle. The typical shape of the TIF for these processes is the W shape.

The sand blasting process and abrasive jet micro-machining are based on the acceleration of abrasive ceramic particles (e.g., Al_2O_3, SiO_2) in a gas stream. The stream is directed towards the surface to be processed at velocities of up to v_{jet} = 200 m/s [3]. A wide range of materials from hard and brittle materials to metals can be processed by these processes. The material removal mechanism is based on small fractures and micro-chippings caused by the particles' impact (see Fig. 12). The particles in common blasting media have a size in the sub-millimeter range, although the particle size distribution can cover a wide spectrum [154].

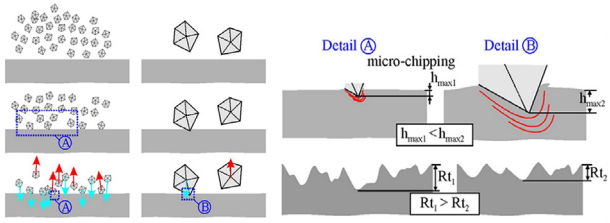

Fig. 12. Influence of the particle size on the material removal and the resulting roughness during sand blasting [40].

In terms of shape adaptability, the influence of a varying standoff distance (SOD) needs to be considered. Oranli et al. [179] varied the SOD during sand blasting of polycarbonate sheets. In a model-based approach, they analyzed the particle velocity for varying air pressures and revealed that a constant impact velocity can be expected for a SOD of 100 to 200 mm. Consequently, even with large differences in structure height, parts with complex shapes can be finished under almost constant conditions (see Fig. 13). However, regarding the morphology after sand blasting, the coverage level slightly decreased with increasing SOD above 200 mm. Besides others, Bouzakis et al. [40] applied sand blasting as a finishing technique for the edge preparation of cutting tools. Different edge geometries were generated by varying the blasting pressure p_b.

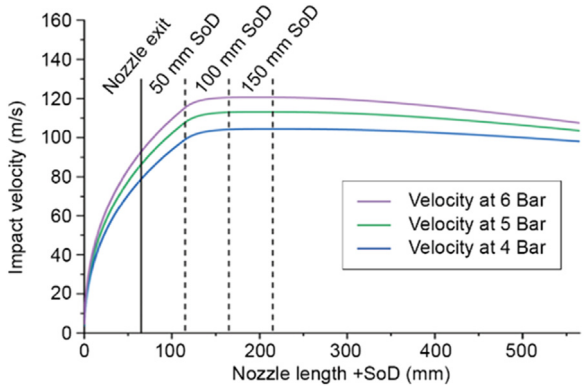

Fig. 13. Dependence of the particle velocity on the air pressure and the standoff distance during sand blasting [179].

Bouzid and Bouaouadja [41] investigated the influence of the impact angle and the blasting time on the resulting surface after sand blasting of soda lime glass. With impact angles lower than 90° (normal to processed surface), the resulting surface roughness continuously decreased. The values almost halved when the angle was changed from 45° to 90°, which indicates that differences in roughness will also occur when finishing complex geometries. Ally et al. [7] observed a reduced MRR for lower impact angles after abrasive jet micro machining of titanium alloys and steels. This is a key challenge for the finishing of complex geometries with regard to shape adaptability. Despite materials for the medical sector [154] or for turbine blades [7] have been sand blasted, publications dealing with the challenges of processing of parts with complex geometries by sand blasting and abrasive jet micro-machining are very rare.

3.3.3. Fluid jet polishing

Fluid jet polishing systems use water instead of air as a carrier fluid [66] or a magnetorheological fluid [202]. The higher density of water means than the velocity of particles is about 30 times lower for a given operating pressure. The drag force is also larger, which means that particles generally follow fluid streamlines and thus reach the surface with an almost tangential velocity [26]. As a result, fluid jet polishing delivers a lower removal rate and finer surface finish than sand blasting, with a tendency to remove high-spatial-frequency waviness from the surface [23], as shown in Fig. 14. Another major difference is the laminar outflow of slurry, whereby the jet remains collimated over a distance of up to 1 m, allowing a small footprint size that is preferable for computer-controlled correction of difficult waviness [282]. The nozzle distance to the surface does not affect the removal rate, which means that fluid jet polishing does not require the complex positioning or force control systems usually employed with compliant polishing tools, as a substantial practical advantage.

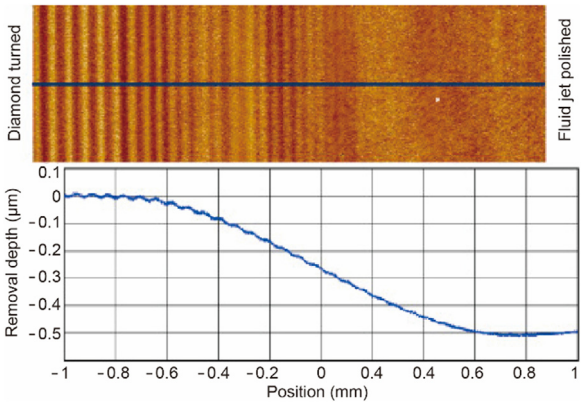

Fig. 14. Removal of high-spatial frequency diamond turning marks by fluid jet polishing with a 1.5 mm diameter nozzle and vertical feed [23].

The relatively low removal rate in fluid jet polishing can be mitigated through a number of approaches. One possible avenue is the use of multiple nozzles [238], which is low-cost but leads to interference in the jet impingement regions and thus generation of complex TIFs. It is also possible to generate cavitation micro-bubbles directly before the fluid escapes the nozzle cavity [21]. In this case, the micro-bubbles cause internal mixing of the slurry to occur, which increases the angle and velocity of particle impacts [21]. Finally, mixing air with the slurry before it escapes the nozzle causes formation of fluid and abrasive particles within an air stream, which increases the outlet velocity together with a partial absorption of the impact energy by the fluid surrounding the particles [87].

The small footprint size in fluid jet polishing means that special attention should be paid to the waviness generation caused by scanning of the TIF with regular patterns [86]. It is however well suited for generation and/or polishing of small features on surfaces, such as micro-channels, as long as the machine and controller settings are optimized [161].

It should however be noted that fluid jet polishing of soft metals and ceramic materials can be challenging, as the abrasive grits tend to either become embedded or cause grains to fall from the ceramic material matrix. This can however be mitigated by operating under submerged jet condition [28].

4. Mechanical processes without material removal

The high relevance of the surface and subsurface characteristics for components with complex geometry drives the application of processes resulting in beneficial surface integrity [103]. Mechanical processes without material removal described here to induce compressive residual stresses, hardness alterations, microstructural changes and in most cases a reduced roughness are referred to as mechanical surface treatment [207]. The most common representatives of mechanical surface treatment are peening processes as well as variants of burnishing processes. They are well established for simple geometry. However, in terms of shape adaptability, they feature characteristic potential as well as limitations, which need to be considered when finishing components with complex shapes.

The TIF for mechanical surface treatment is characterized by continuous (burnishing) or discontinuous (peening) contact of mechanical load-imposing bodies with the workpiece surface. Given the small TIF, the processes can be applied to workpieces with small and large dimensions. The accessibility of the surface to the peening media or the tool can be of limiting character for highly complex geometries of the part.

The high mechanical loads lead to localized plastic deformation of the workpiece surface and to changes in the subsurface characteristics below the load-imposing body. The projected area of the contact is typically below 2 mm^2, leading to surface coverage ratios several orders of magnitude smaller than 1. The plastic deformation of individual contacts results in an inhomogeneous modification of the topography and the subsurface characteristics. This is why very high overlapping rates of tool footprints are selected for burnishing and machine hammer peening to achieve a homogeneous processing result.

4.1. Peening processes

In mechanical surface treatment, peening processes are characterized by impulse-like impact of the peening media to the peened component. The peening media can be solid (shot peening), liquid (water jet peening), or pulsed laser-induced cavitation (laser shock peening, see Section 6.2.2) [216]. Peening can be performed using loose media or a guided tool (machine hammer peening). All of these finishing processes can be applied to complex shapes with limitations regarding the accessibility of the body impacting to the surface.

4.1.1. Shot peening

In shot peening, solid bodies (shots) are accelerated and hit the processed surface in free flight. In terms of shape adaptability, the major influencing factors during shot peening of complex geometries are the standoff distance (SOD, distance of free flight) and the impact angle β_i. For complex surfaces [275] and a fixed position of the nozzle, these variables change during the process.

Fuhr et al. [74] analyzed the relevance of the impact angle on the surface and subsurface properties of Ti-6Al-4V. For a variation of the impact angle between β_i = 90° and β_i = 30°, they concluded that the effect on the resulting roughness can be neglected. Only at very high overlapping ratios of 1200 %, a moderately reduced roughness at an impact angle of 90° has been observed. It has to be noted that all shot peened surfaces showed higher roughness compared to the as-machined (ground) state of the specimens. For additively manufactured Ti-6Al-4V, they observed a reduction of the initially very high roughness ($Rz > 150$ µm) to $Rz = 100$ µm. While the robustness of the resulting surface roughness against variations of the impact angle indicates shape-adaptability over a wide range, the subsurface characteristics change at comparably low impact angles. In fatigue test, the authors reveal slightly higher fatigue strength for samples which were shot peened with an impact angle of 45° and below. At a constant peening intensity, the increasing shear loads at lower impact angles increase the resulting compressive stress, dislocation density and material flow, leading to higher fatigue strength.

Concerning the relevance of the standoff distance on the shape adaptability, Khany et al. [116] varied the SOD in a range between 120 mm to 155 mm during shot peening of a low carbon steel. Even though the authors describes that the S/N ratio (alternating stress versus the number of cycles) of the shot peened specimen improved slightly when a low SOD was selected, the effect was still very small. In addition, SOD varied within a range of 25 mm during the investigations. Considering the negligible influence of the variation of SOD on the processing result, it can be noted that shot peening has a high shape adaptability. This is confirmed by Hennig et al. [94] in shot peening of Ti6246 blisks (Fig. 15). By adapting the nozzle design and the nozzle path using a 3D-model of the component, they made use

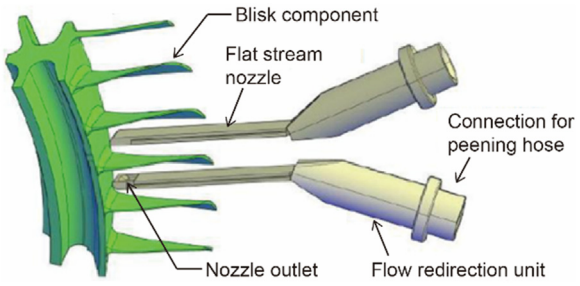

Fig. 15. Shot peening for aerofoil treatment of blisk assemblies [94].

of the robustness of the process e.g., in terms of SOD to successfully finish complex geometries. Considering application of shot peening for shape-adaptive finishing, the common increase in roughness and the expected rounding of pointed structures due to plastic deformation should be emphasized.

4.1.2. Water jet peening

In water jet peening [236], the high frequent impact of water droplets causes plastic deformation in the surface and subsurface layers. For this purpose, water pressures of more than 100 MPa are applied. In contrast to the conditions for fluid jet polishing (Section 3.3.3), no abrasive particles are added into the water. However, material removal can be observed even for water jet peening without abrasive particles. In water cavitation jet peening [15,151], the jet is injected into a water-filled chamber causing the formation and collapse of bubbles accompanied with cavitation effects.

In water jet peening applied for mechanical surface treatment without material removal, the nozzle geometry (nozzle diameter d_n and nozzle angle α) and the standoff distance SOD are decisive for the size of the typically round or elliptical shape of the water jet (Fig. 16, left). The structure of the jet (Fig. 16, right) is subdivided into three regions [218]. In the initial region, the continuous flow of the solid core causes constant axial pressure, which is not sufficient to induce plastic deformation of the workpiece surface. This region is not suitable for mechanical surface treatment. In the transition region (also referred to as main region or droplet flow region), the jet falls into separate water droplets which, at impact, cause local plastic deformation due to higher dynamic pressure compared to the solid core. In the final region, jet diffusion causes a reduction of the droplet size and thus insufficient impact pressure of the single droplets. With regard to the treatment of parts with complex geometry, this indicates that for successful processing, the distance between nozzle and workpiece must always stay within the transition region. Furthermore, the peening angle may change during water jet peening of complex parts. The influence of variations of these parameters are discussed below in more detail.

In an experimental study using a 6063-T6 aluminum alloy, Balaji and Jeyapoovan [14] identified the standoff distance and the water pressure as the decisive factors for the achievable microhardness. For the resulting surface roughness, the interaction between the standoff distance and the traverse rate was revealed as the major influencing factor. This means that the standoff distance may not be varied in wide ranges when finishing parts with complex shapes. Ming et al. [159] addressed the influence of the standoff distance in more detail and revealed a maximum of compressive residual stresses at the 30 mm standoff distance. Higher and lower standoff distances during water jet peening of 316 L steel led to a drop of the compressive residual stresses. For changes of the standoff distance of less than 5 mm, only a small decrease of the resulting surface and subsurface characteristics was observed. This indicates that parts with complex geometries featuring height differences of less than 5 mm can be water jet peened without significant changes of the processing result. For water jet peening of helical gears, Qin et al. [188] analyzed the influence of the impact angle on the impact pressure along the cross-section of the jet. The maximum impact pressure was found in the center of the jet for impact angles from 0° to 90° and there was no influence of the angle on the maximum pressure. However, at the lowest and highest impact angle (0° and 90°) the impact pressure dropped much earlier and more strongly with increasing distance from the center of the jet. For a 0° impact angle, this resulted in less pronounced residual compressive stresses indicating that processing complex surfaces, a variation of the impact angle may lead to inhomogeneous residual stress states.

4.1.3. Machine hammer peening

In machine hammer peening [207], the tip of a plunger is accelerated towards the processed surface pneumatically [191], electromagnetically [34] (Fig. 17), mechanically [148], sonotrode driven, or by piezoelectric effects [138].

For machine hammer peening, the impact angle can be varied by means of the angle of attack (perpendicular to feed direction) and the tilt angle (parallel to the feed direction). For a constant distance t between the plunger tip and the workpiece surface. Bleicher et al. [35] simulated processing complex geometries by deliberately varying the impact angle β_i to analyze the process forces. At $\beta_i = 90°$, maximum forces were observed which decreased with decreasing β_i. A non-linear correlation characterized by a moderate drop of the axial forces by less than 15% for impact angles down to $\beta_i = 75°$. In the range of $75° > \beta_i > 65°$, a sharp decline of the axial forces down to 35% of the value for perpendicular impact is observed. This value stayed constant for a further decrease of the impact angle down to $\beta_i = 45°$. At the same time, the radial forces increased with declining impact angle and reached the same level as the axial forces at $\beta_i = 45°$.

Wied [255] analyzed the effect of the angle of impact for machine hammer peening of ZnAlCu3. A deviation from an ideal perpendicular impact ($\beta_i = 90°$) resulted in a less pronounced smoothing of the surface. The same observation was made by Bleicher et al. [35], who analyzed the surface roughness of machine hammer peened AISI D2 steel in terms of *Ra* for different impact angles and varied peening distance *t*. For the hardened state, the surface roughness after machine hammer peening increased by 40-145% depending on the peening distance. Interestingly, the opposite effect was observed for the same material in a soft (unhardened) state. Here, an impact angle of $\beta_i = 60°$ led to an up to 50% reduced *Ra*-value. The authors explained these observations by the higher orthogonal forces required to flatten the roughness peaks from pre-machining for hard materials. Mannens et al. [150] performed machine hammer peening tests using martensitic AISI CA6-NM as the workpiece material. In agreement with the results of Bleicher et al., the authors were able to determine

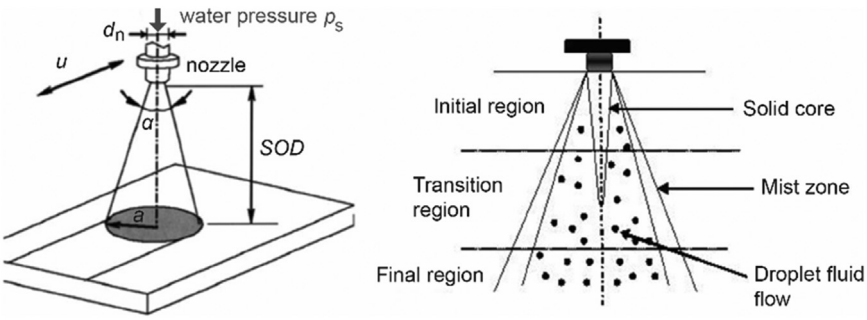

Fig. 16. Effective variables of a water jet peening and change in jet structure with standoff distance [218,236].

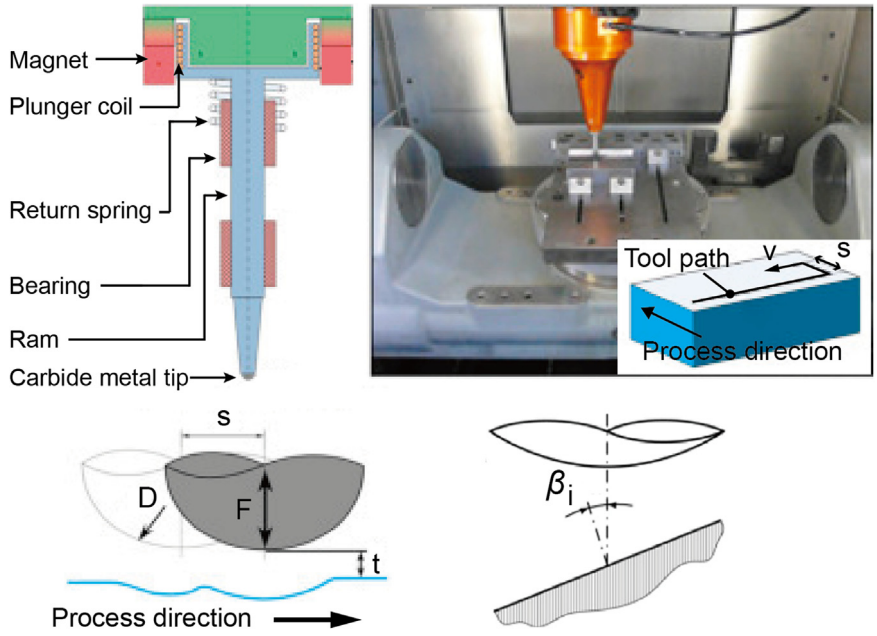

Fig. 17. Design and experimental setup for machine hammer peening with an electro-magnetic actuator [34].

an increase in surface roughness with decreasing impact angle for this high-hardness material state. This indicates that for finishing components with complex geometry, the surface finish will vary at different impact angles. Considering the high orthogonal forces required to flatten the surface of harder materials, impact angles of $\beta_i > 75°$ offer a stable process window without significant loss of force.

4.2. Burnishing processes

According to Schulze et al. [207], burnishing covers a number of processes such as roller burnishing, deep rolling, and diamond smoothing, all being characterized by a guided tool. Deep rolling differs from roller burnishing in such a way that the process is designed to induce more extensive plastic deformation. Burnishing is furthermore subdivided into ball burnishing and roller burnishing depending on the geometry of the used tool. Tool concepts featuring mechanical bearing (springs) as well as hydrostatic bearing with tool holders designed to realize a certain stroke are available, which has a direct effect on the shape adaptability of the processes described below. In addition, it should be noted for all burnishing processes that the diameter of the tool used is a limiting factor for the processing of complex geometries. Tools with a defined radius, typically in the range of a few millimeters are commercially available. The smallest diameter available for diamond smoothing is 0.4 mm. These dimensions do not allow structures with smaller radii or angles to be processed without adversely changing shape. There is no established technology to specifically process complex microstructures with these burnishing or deep rolling tools.

4.2.1. Roller and ball burnishing

In tool concepts for roller burnishing and ball burnishing with fixed burnishing body, the burnishing force is a result of the defined travel of the tool in the normal direction of the surface to be burnished (path dependent). Without adaptation of the tool path during the process, a varying distance between the center of the tool and the processed surfaces leads to a variation of the burnishing force. In terms of shape adaptability, even minor deviations from ideally flat surfaces would result in locally varying surface and subsurface characteristics. Yaman et al. [264] presented results from roller burnishing experiments using additively manufactured Inconel 718 as a workpiece material. Despite the limited stroke of the tool, the process was suitable to reduce surface roughness from Ra = 15 µm (as built) to Ra = 0.32 µm after burnishing. Similar results were presented by Rotella et al. [201] for roller burnishing of stainless steel. This indicates that at least the height differences in the initial roughness of AM-parts allow for homogeneous burnishing. Considering the track depth for single track burnishing experiments, the indentation depth is usually set to 50-150 µm (e.g., [274]) and thus higher than common initial roughness values. The same applies to diamond smoothing, where a fixed diamond travels over the surface to be smoothed with comparably low mechanical loads. Liborius et al. [137] quantified the surface roughness after diamond smoothing with a tool diameter of 2 mm and the forces at 200 N and below by means of the valley void volume. At low feeds and high forces, the valley void volume was reduced to 0.1 ml/m^2 which led to more pronounced fretting effects testing the diamond smoothed thermally sprayed Fe17Cr2Ni0.2C coating.

There are a few references dealing with mechanical bearing burnishing systems with springs for finishing complex shapes. In the investigation of the surface integrity of cylindrical aluminum workpieces, Harish and Shivalingappa [89] observed a more pronounced effect of roller burnishing at identical burnishing forces. However, the exact tool diameters were not disclosed, and small deviations of the ball and the roller might have caused the different results in terms of roughness and strain hardening. Lopez de Lacalle et al. [144] used a burnishing system with hydrostatic bearing system to improve the roughness of molds and dies with freeform surfaces (see Fig. 18). It was found that burnishing led to similar finish to hand polishing with a roughness of Ra = 0.18 µm.

For complex shapes, adaptation of the tool path is required. Tsuchida et al. [239] presented two different approaches to compensate for the shape change of the workpiece in ultrasonic vibration assisted burnishing of zirconia ceramic. A flexible stage was used to keep the mechanical load constant and was shown to lead to beneficial surface finishing. Working without the flexible stage but with a rotating burnishing tool resulted in reduced roughness, regardless of the ultrasonic excitation of the tool. The tool concepts with springs thus have been proven to be suitable for finishing components with complex shapes. The aforementioned limitations regarding the diameter of the tools and the accessibility of the surface to be finished however remain.

4.2.2. Deep rolling

To induce high compressive residual stresses [61], hardness alterations [1,157], and microstructural transformations [43,156], hydrostatic deep rolling tools or mechanically mounted tools [181,289] are applied. For hydrostatic deep rolling tools, the metalworking fluid of the machine tool is applied to the deep rolling ball at high pressures. The stroke of the ball holder available with hydrostatic deep rolling tools, which is in the range of several millimeters, was used by Klocke and Mader [120] as well as Bäcker et al. [13] to finish turbine blades

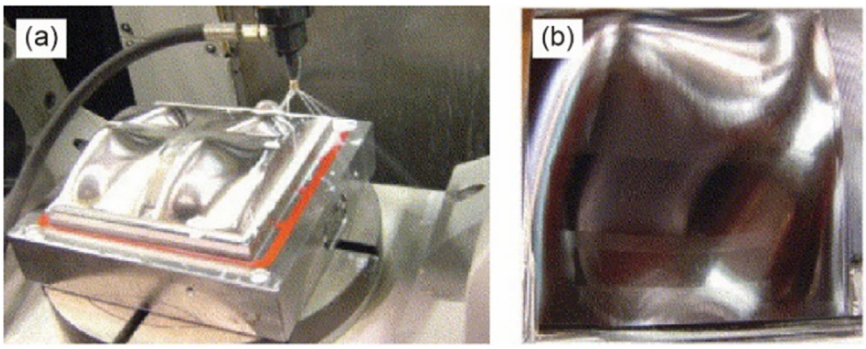

Fig. 18. Ball burnishing of a mold made of H13 tempered steel: (a) details of the burnishing setup, (b) one of the burnished surfaces [144].

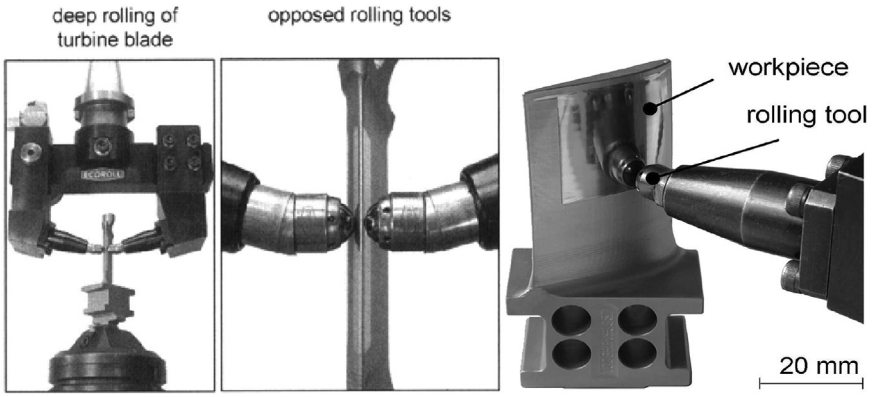

Fig. 19. Deep rolling of turbine blades [120].

(Fig. 19). In experimental and numerical investigations, they observed homogeneous material modifications along the processed surface of the blades.

The influence of a varying distance between the hydrostatic deep rolling tools and the processed surface was furthermore investigated by the Leibniz-IWT in Bremen. A cylindrical workpiece made of quenched and tempered AISI 4140 was milled to generate an eccentricity of max. 4 mm (Fig. 20). The part was deep rolled on a turning lathe using a hydrostatic deep rolling tool with a ball diameter of d_b = 6 mm and a force of F_r = 1130 N at a feed of f = 0.1 mm and a rolling speed of v_r = 50 m/min. This set-up led to a quick variation of the distance between the fixed position of the tool holder and the processed surface. The stroke of the ball holder allowed tracking of the deep rolling ball for up to 3.5 mm. The resulting surface residual stresses indicated that only a slight decrease of the compressive residual stresses was observed for the area exposed to increasing distance between the tool holder and the processed surface. This indicates a moderate effect when deep rolling complex geometries with hydrostatic deep rolling tools. The general design of mechanically mounted deep rolling tools is identical with the tools applied in ball or roller burnishing. Thus, the potential and limitations discussed in Section 4.2.1 apply to deep rolling with those tools.

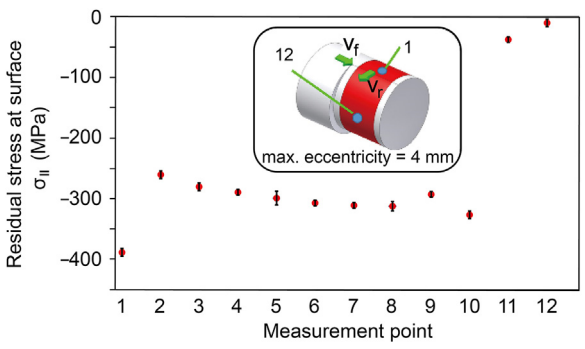

Fig. 20. Residual surface stresses of a deep rolled sample with 4 mm eccentricity.

5. Chemical Processes

Surface finishing can also be performed via chemical processes. Unlike mechanical processes, where force (stress)-driven material removal or redistribution occurs, in chemical processes, however, chemical reaction is the dominant factor for material removal (no redistribution) with limited or no presence of force (stress). Chemical reactions can be realized by using chemical solutions, electrolyte, and plasma. This section reviews major chemical processes which are useable (or potentially useable) for shape-adaptive surface finishing of complex shapes.

5.1. Solution-based chemical polishing

Solution-based chemical polishing (SCP) is an effective method to improve the surface quality of metal parts that have complex geometries. In recent years, it has attracted researchers to use chemical solutions for polishing to enhance the surface quality of additive manufactured parts [17]. General process steps of chemical polishing are presented in Fig. 21(a). It is necessary to clean the part's surface to remove contamination and undesirable oxides before immersing the entire part in chemical solutions. The metal surface dissolves into metal ions, and the ions diffuse in the solution. When the metal dissolution rate is faster than the ion diffusion rate, metal ions are concentrated in the concave, and the density of cations (mainly hydrogen ions (H^+)) in the solution decreases in the concaves, as shown in Fig. 21(b). As the etching rate at the convex parts is greater than that at the concave parts, a smooth surface is gradually formed [111]. It is easily seen from Fig. 21(a) that the SCR of solution-based chemical polishing can reach 1. The TIF will be determined by the local curvature of the surface as well as the chemical reactivity influenced by factors such as solution concentration and temperature.

Depending on the material of the parts, the solution components are different. For example, phosphoric, nitric, and hydrochloric acids-based solutions are employed for the chemical polishing of stainless steel [85,240]. Aluminum can be chemically polished by phosphoric-sulphuric-nitric acid. Depositing a certain amount of copper on

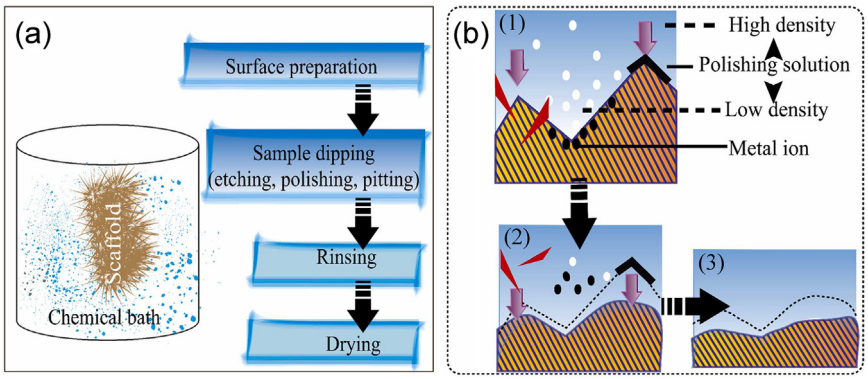

Fig. 21. (a) Process steps of chemical polishing, and (b) its material removal mechanism [17].

aluminum can improve the polished surface quality [53]. Adding nanostructured media (microemulsion) to the acid can greatly reduce the surface roughness of aluminum [166]. The acidic solutions containing HF and HNO_3 with different HF/HNO_3 molar ratio are used for chemically polishing Ti-6Al-4V [149,249]. It was found that by combining isostatic pressure with chemical polishing, the fatigue limit was significantly increased [10]. For the polishing of copper, not only acids-based solutions [68], but also weak alkaline solutions can be used [108].

To chemically polish 3D parts printed from polymer filament, organic solvents are the suitable solutions. Instead of immersing the parts into the solutions, chemical vapor was used to eliminate the layer grooves on the part. By the influence of gravity and liquid surface tension, the groove-like structures were slowly dissolved and smoothed. As the printing material changes, the choice of chemical vapor also varies. Acetone vapor was used to polish acrylonitrile butadiene styrene (ABS) [92], and dichloromethane vapor to polish polyethylene terephthalate-glycol [145]. The longer the part is immersed in the chemical vapor, the more material is dissolved, which may finally cause dimension change of the part. In addition, vaporized solvent does not support selective polishing and may cause the loss of small features. Fig. 22(b) shows an ABS dog model polished with acetone vapor. Although a smoother surface is obtained than before polishing (Fig. 22(a)), the lines around the eyes of the dog disappeared. To overcome this drawback, Takagishi and Umezu [227] developed a pen-style device filled with a chemical capable of dissolving the materials selectively. By controlling the movement of this pen-style device, it dissolves the convex parts of the layer grooves on the model surface, subsequently filling the concave parts and smoothing the layer grooves. With this pen-style device, localized removal of layer grooves on 3D printed surfaces is

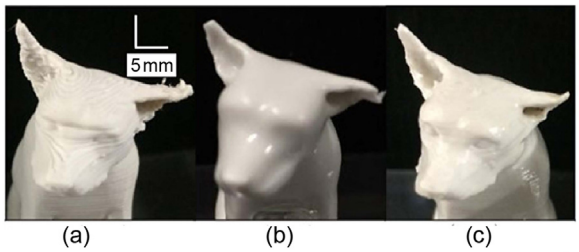

Fig. 22. Dog 3D printing models: (a) without surface finishing, (b) with acetone vapor finishing, and (c) pen-style finishing [227].

achievable while keeping solvent usage at a safe level. Fig. 22(c) shows an ABS dog model polished with the pen-style device filled with acetone. It improved the surface roughness while maintaining the detailed structures around the eyes by performing selective treatment.

5.2. Dry electropolishing

Dry electropolishing (DEP), recently developed by GPAINNVA [80], utilizes electrolyte-containing polymeric spheres as electropolishing media that can conduct electricity and remove the oxides produced during electropolishing. The combination of electrical flow and workpiece movement within the media induces ion exchange, selectively removing material from the peaks of a rough surface, as shown in Fig. 23. Since no liquid is used as electrolyte, dry electropolishing achieves less chemical alteration to workpiece, significantly reduces chemical waste, and provides a better working environment compared to solution-based chemical

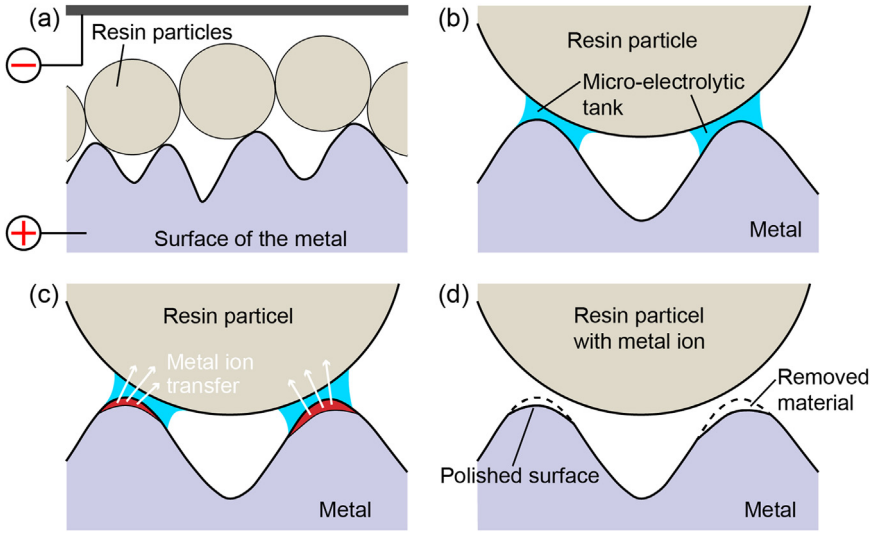

Fig. 23. Mechanisms of dry electropolishing: (a) point contact between a surface and resin particles; (b) micro-electrolytic cell formation around collision points; (c) anodic reaction occurrence and metal ions transfer to resin particles; (d) peak removal and surface smoothing [158].

polishing and wet electropolishing. Furthermore, the edge rounding problem, happening in most pressure-based polishing processes, is insignificant in DEP. The access to corners and holes, that are difficult to access in mechanical processing, becomes easier. The workpiece may be rotated during the polishing process, allowing the inner surface of a tubular product to be polished as well [257]. Similar to solution-based chemical polishing, dry electropolishing has an SCR of 1. The TIF is determined by the local curvature of the surface, as well as the size of the electrolyte-containing polymeric spheres and the applied voltage.

Dry electropolishing has been validated in polishing several materials including Inconel 718 [257], BT-6 titanium alloy [124], Ti-Al-V alloy [269], cobalt-chrome [193], WC-CO cemented carbide [196], and 316L stainless steel [192]. Fig. 24 shows a comparison of a BT-6 titanium alloy compressor blade before and after dry electropolishing. The surface roughness was reduced from 0.32 to 0.04 μm *Ra* [124]. However, dry electropolishing was found not able to reduce *Rz* as much for surfaces produced by laser powder bed fusion because it was difficult to remove all the partially melted particles from the surface [192]. Additionally, the effectiveness for improving the fatigue limit depends on the processed materials. For example, dry electropolishing enhanced the fatigue limit of Ti-Al-V alloy [269], while this was not the case for 316L stainless steel [192].

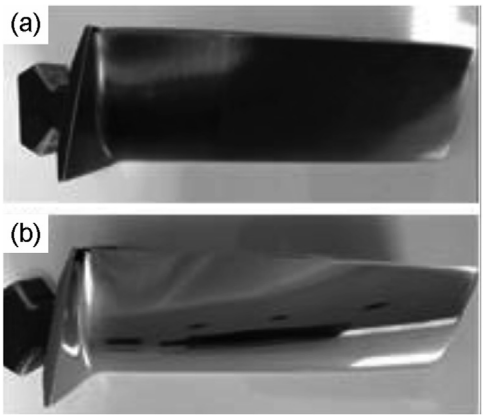

Fig. 24. Compressor blade made of BT-6 titanium alloy (a) before and (b) after dry electropolishing [124].

5.3. Plasma-assisted polishing

Plasma-assisted polishing (PAP) is a dry polishing method to achieve damage-free surface on hard-to-machine materials, which combines surface modification using plasma irradiation and removal of modified layers using ultra-low polishing pressure or soft abrasives [219]. A schematic of the experimental setup for PAP is shown in Fig. 25(a). In general, it consists of two parts, plasma irradiation and mechanical removal. The plasma jet, consisting of free radicals and active species, is generated by applying a radio frequency (RF) electric power to dissociate the reactive gas, impinging the surface and reacting with the material to form modified layers [60]. Whereas in the mechanical removal part, the modified layer is removed by a polishing tool with soft abrasives. The specimen is placed on a linear stage, and the PAP is conducted via two sequential steps: surface modification by plasma irradiation and dry polishing by abrasives, as detailed in Fig. 25(b).

Different from hot plasma (T_i in the range of 10^4~10^5 K), which can effectively reduce mechanical strength and hardness of materials via the thermal softening effect, the cold plasma (T_i in the range of 10^3 K) adopted in PAP involves physical and chemical effects but less thermal effects. It operates based on chemical reactions between the active radicals in the plasma and surface material to improve material removal rate and surface integrity [140]. In PAP, chemical reactions in material modification need to be carefully designed and optimized to achieve the total process performance. Given the thickness of the modification layer is in the level of tens of nanometers, PAP is mainly used for finishing high-accuracy parts.

In the past decade, PAP has been applied to processing a variety of hard-to-machine materials including silicon carbide [59], aluminum nitride [220], gallium nitride [57], sapphire [19], and diamond [141]. For example, it was used to surface finishing of gallium nitride, where the surface material is modified into gallium fluoride (GaF_3) via CF_4-plasma irradiation, then the modified layer (GaF_3) is removed by dry polishing using a CeO_2 grindstone. This avoids the preferential etching or oxidation of the dislocation sites that occur in slurry polishing, and an ultra-smooth (*Sq* <0.1 nm) surface was generated [57]. Furthermore, results demonstrated that the cold plasma could oxidize silicon carbide and turn it into silicon dioxide, through which the surface hardness significantly decreases from 37.4 to 4.5 GPa [59]. The silicon dioxide on the modified layer can be easily removed by a resin-bonded CeO_2 grinding stone and a scratch-free surface with *Sq* of 0.69 nm was obtained [58]. The surface topographies of the plasma etched, and PAP processed SiC surfaces are compared in Fig. 26, the latter showing a distinctly better surface quality. For polishing single-crystal diamond, the plasma irradiation and polishing plate induce O radicals and frictional temperature as the catalyst effect to accelerate the mechanically induced graphitization during PAP to achieve anisotropic removal [263]. The material removal rate was 10 times greater than that of conventional polishing, and surface roughness of 0.13 nm *Sq* was obtained [263]. However, most available literature on PAP is on surface finishing of planar wafers. Application of PAP to freeform surface finishing requires precision control of the MRR irrespective of the surface curvature.

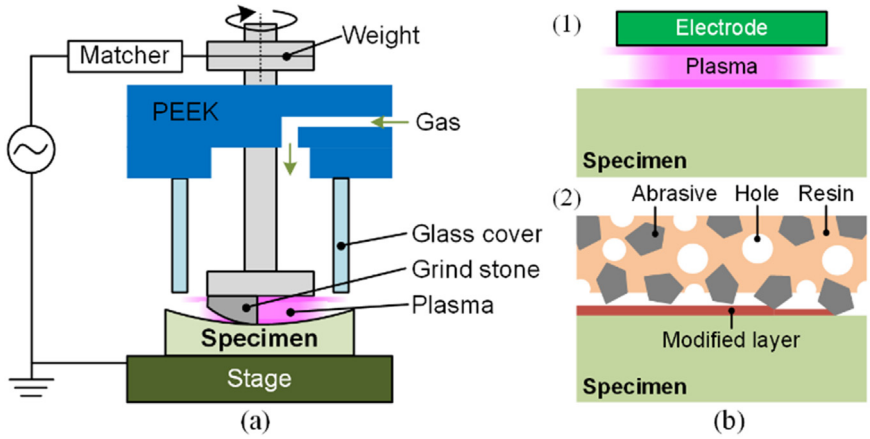

Fig. 25. (a) Schematic of PAP setup [58]; (b) mechanism of PAP [219].

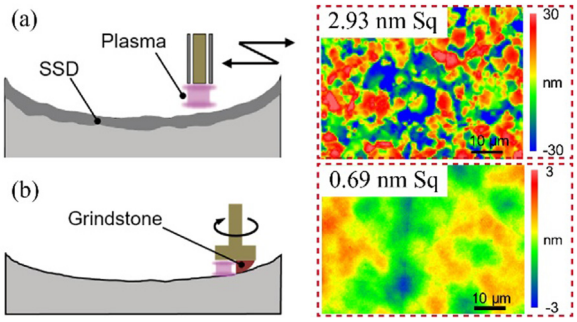

Fig. 26. Schematics and 3D topographies of the (a) plasma etched, and (b) plasma-assisted-polished SiC surfaces [58].

6. Physical processes

This section explores a variety of physical processes used for surface finishing, such as ion beam figuring, large-area electron beam irradiation, laser processes, and electric discharge polishing. The primary emphasis lies in elucidating the material removal and shape control mechanisms inherent to each of these processes. Similarly to chemical processes, physical processes do not involve mechanical force (stress), thus can be used for processing various difficult-to-machine materials without the need to consider the material hardness and brittleness.

6.1. Ion beam figuring

Ion beam figuring (IBF) draws ions from plasma, accelerates them with high voltage, and irradiates them onto a target to process the material using their collision energy, as shown in Fig. 27. The IBF method adjusts the dwell time to realize the desired surface topography. Since processing is performed by irradiating ions, it is possible to process on an atomic scale in principle. Excelling in minimizing damage, IBF is effective across a variety of materials irrespective of electrical conductivity, including optical glass, metals, semiconductors, and plastics. Its applications are diverse, ranging from the creation of intricate optical components to the development of advanced X-ray mirrors [77].

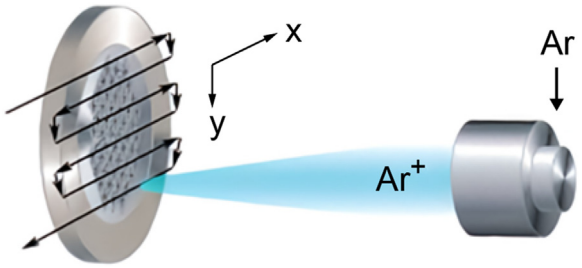

Fig. 27. Schematic of ion beam figuring principle [273].

The early challenges of IBF are noteworthy. In the 1990s, IBF emerged as a technology in optical manufacturing, overcoming the limitations of traditional machining. The research by Schindler et al. [205] in 2001 showed the intricate material removal process in IBF, emphasizing its reliance on ion sputtering and precise positioning. A previous comprehensive review [6] explored IBF in comparison with other electrical, physical, and chemical machining methods. This paper indicates that IBF processes rarely exceed surface temperatures of 400 K, while other processes like laser beam machining can reach 10,000 to 30,000 K. Also, IBF relies on ion impact to remove surface atoms, whereas plasma discharge machining involves chemical reactions at atmospheric pressure. Ion beam processes have significantly higher energy levels compared to plasma processes.

The increasing demand for precision, particularly in the realm of ultra-precision optics used in lithography, urged advancements in IBF algorithms and techniques after 2009. Notably, Wu et al. [71] developed algorithms to achieve nano-scale surface accuracy and craft low-gradient mirrors. Jiao et al. [107] managed to achieve surface errors less than 1/100th of a wavelength on SiC and Zerodur samples. To expand this technology, Arnold et al. [11] pioneered IBF and atmospheric plasma jet technologies for aspherical optics in synchrotron and X-ray applications. IBF demonstrated remarkable accuracy at sub-nanometer order across various materials. Recent advancements have further pushed the boundaries of this technology. Wang et al. [253] addressed post-IBF roughness in Si with an optimized vacuum pumping scheme, achieving surface smoothness. Du et al. [62] combined IBF with polishing to efficiently remove turning marks on aluminum, resulting in low roughness. IBF has also significantly enhanced the properties of sapphire [146]. The surface roughness of high-purity sapphire has been reduced to improve infrared transmission properties. Current research focuses on factors such as particle energy, weight ratio, temperature, and angle of incidence to further optimize surface smoothness and address microdefects. However, due to the small spot size of the ion beam, the SCR of the IBF process is usually very small ($<<1$).

6.2. Large-area electron beam irradiation

Electron beam (EB) is a type of energy beam that accelerates electrons and causes a physical collision on the surface to melt or evaporate the material. Large-area EB irradiation has been demonstrated as a highly efficient method of polishing metal mold surfaces [168]. The SCR of this method is large (=1 or <1). Using large-area EB irradiation, Okada et al. [177] polished Ti by closely controlling the irradiation conditions, while Tokunaga et al. [234] took advantage of the low thermal conductivity of cast alloy, raising the surface temperature to the melting point in just a few minutes to achieve a smooth surface. The Ti alloys after EB processing were found to have dramatically improved wear and corrosion resistance as well as heat resistance, expanding their lifespan in aerospace and medical applications.

Large-area EB irradiation is also effective in polishing steels and has been applied in the surface finishing of molds with various shapes. Okada et al. [176] treated stainless steel for surgical tools and jigs using the large-area EB irradiation. The surface quality and blood repellency were both improved. Uno et al. [242] used 60 mm-diameter electron beams to irradiate mold steel (NAK80). This method reduced surface roughness from 6 μm *Rz* to less than 1 μm *Rz* in just a few minutes. Fig. 28 shows the effect of EB polishing on an electrical discharge machined surface of mold steel. The surface became distinctly smoother when an optimal energy density was used. In addition, Murray et al. [167] repaired electrical charge-induced cracks in AISI 310 stainless steel. They also smoothed intricate molds with micro pillar structures, significantly refining both the microstructure and substrate surfaces [168]. Recent research addresses surface smoothing of additively manufactured parts, with promising surfaces devoid of oxide layers. Recently, Shinonaga et al. [213] explored edge filleting for convex parts, and demonstrated the potential for precise shaping by EB irradiation without part deformation.

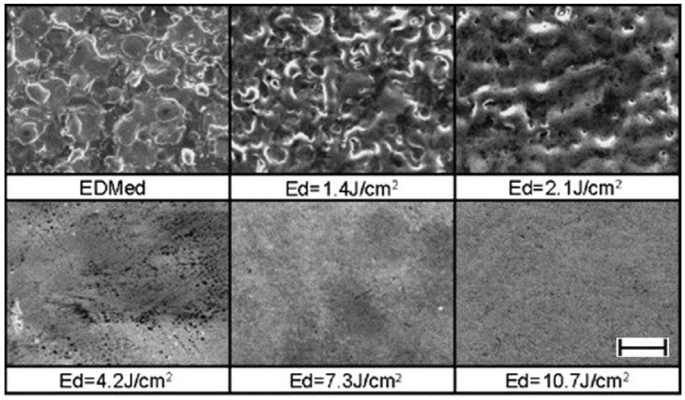

Fig. 28. Large-area EB irradiated mold steel surfaces for various energy densities after 30 times irradiation [243]. (The scale bar is 50 μm)

6.3. Laser processes

6.3.1. Laser polishing

Laser polishing is a technology for smoothing surfaces by gently melting or removing an ultra-thin layer of material, a schematic of the former of which is shown in Fig. 29. This non-contact process, which utilizes a precisely controlled laser beam, excels in precision, efficiency, and adaptability to various shapes, making it applicable across a wide range of industries.

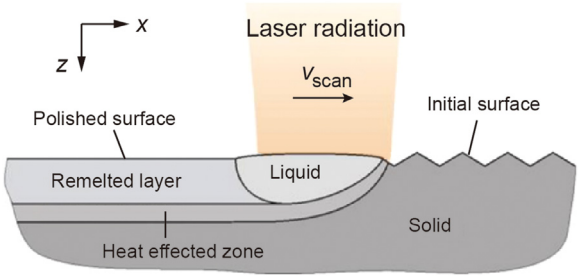

Fig. 29. Schematic of laser polishing by remelting a thin surface layer with continuous laser radiation [233].

Continuous wave lasers, with wavelengths exceeding 1 µm, cause the material to absorb energy, leading to surface melting or evaporation. The choice between Nd:YAG, fiber, and CO_2 lasers depends on the material, shape, and desired outcome. Zhao et al. [280] reported that a CO_2 laser removed cracks in fused silica, achieving higher processing speed and quality compared to traditional methods. Fiber laser polishing of Ti-6Al-4V, as reported by Pfefferkorn et al. [183] reduced surface roughness by 72%. Eckert et al. [64] unveiled the mechanism of surface smoothing through melting and evaporation.

In terms of microstructural transformations, Telmir et al. [232] conducted laser polishing on H11 tool steel, which led to grain refinement, increased hardness, and reduced carbon concentration, but introduced high tensile stresses. Liu et al. [139] reported that UV laser polishing of CVD diamonds via precise material removal and achieved surfaces with 8 nm *Ra* while preserving optical quality.

Ultrashort pulse lasers, such as femtosecond and picosecond lasers, are suited for polishing hard and brittle materials like sapphire. Non-thermal ablation is a process that removes material by a non-linear absorption process without generating significant heat. Taylor et al. [231] focused on polishing germanium using a femtosecond laser, exploring parameters for non-thermal ablation. Schafer et al. [203] achieved a surface of 20 nm *Sq* on lithium niobate using ultrashort laser pulses. Qian et al. [187] investigated laser polishing for coating films, highlighting the role of roughness and microstructure in oxidation resistance. Chen et al. [49] pioneered the simultaneous creation of shapes and surface finishing on glass using a femtosecond laser. They used a model to predict the interaction process, including plasma generation and surface temperature, allowing for precise control over material removal and surface finishing. Tan et al. [229] proposed an innovative method for polishing glass micro lens arrays at nano/microscale, which efficiently creates ultrasmooth surfaces without damaging shape accuracy.

In the field of additive manufacturing, laser polishing has been used to enhance surface quality and reduce roughness in various complex parts, as shown in Fig. 30. Rosa et al. [200] demonstrated improved surface quality on additive-manufactured parts. Marimuthu et al. [152] developed a model to understand melt pool dynamics and achieved a significant reduction in roughness. Fang et al. [69] reduced the surface roughness of Inconel 718 from 7 µm to less than 0.1 µm *Ra*. Yung et al. [272] enhanced the surface quality and hardness of CoCr with dynamic laser focus adjustment. Wan et al. [246] reduced the surface roughness of AlSi10Mg by 68.3% to 7.1 μm *Sa*. Cvijanovic et al. [54] achieved up to a 70% reduction in *Sa* on IN-738 parts through Nd:YAG laser polishing. Kobayashi et al. [122] proposed a surface finishing method for steel molds by using a picosecond pulsed laser. The process involves the steps of surface flattening by removing the surface asperity via laser ablation and generating nanoscale laser-induced periodic surface structures (LIPSS) on the flattened surface.

6.3.2. Laser shock peening

Laser shock peening (LSP) is based on the generation of elastic shock waves [182,215]. The vaporization of the first atomic layers of an opaque absorption layer due to the interaction with the laser pulse produces a plasma plume whose expansion is limited by application of a thin film of a transparent medium. The plasma causes high surface pressure and recoil effects. As a result, the surface and subsurface layers are plastically deformed, and compressive residual stresses are induced [230]. The spot diameter is usually in the millimeter range with a homogeneous distribution of the pressure along the beam diameter [42]. With respect to shape adaptability, the dependence of spot radius and laser intensity on distance from the lens must be considered. As shown in Fig. 31, laser intensity increases as spot radius decreases. Although the increase in intensity with decreasing spot radius is generally quite steep, it is a matter of distance variations in the range of several millimeters. As a result, the process capability can be classified as robust when processing complex surfaces with such height differences [212].

Research dating back to the 1990s laid the foundation for this technology, and now heavy industries are reaping the benefits. LSP is effective especially for large, lightweight magnesium components manufactured through wire arc directed energy deposition [134]. Recent advancements, such as droplet confinement for high-temperature LSP and 3D gradient LSP for crafting multi-scale hydrophobic surfaces, hold immense promise for a variety of applications [278]. The study by Pan et al. [180] demonstrated that the effect of LSP on microstructure can increase fatigue strength by up to 37 %. This creates lighter and stronger components in a variety of industries.

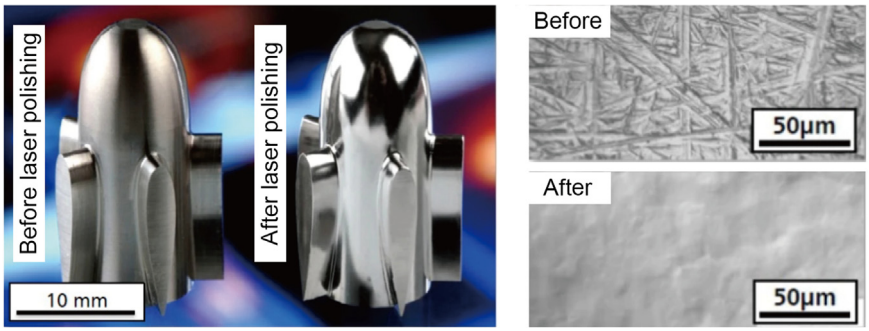

Fig. 30. Example of laser polishing for ventricular assist devices [79].

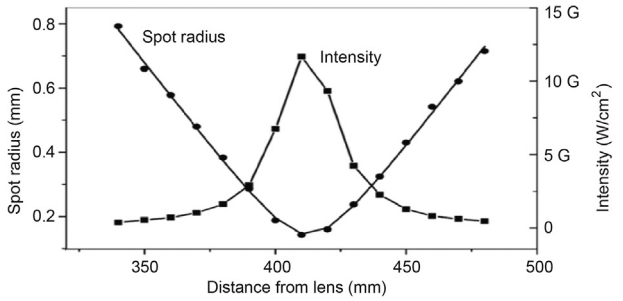

Fig. 31. Variation of laser spot radius and intensity as a function of distance from the focusing lens [221].

6.3.3. Laser recovery

Laser recovery is a surface finishing method for single-crystal materials that eliminates subsurface defects generated in pre-processing steps such as cutting, grinding, and polishing. The damaged areas are repaired using a laser beam, finally revealing a uniform surface with a perfect crystalline structure. A study by Yan et al. [266] focused on the possibilities offered by laser recovery of silicon single crystals. Their nanosecond pulsed Nd:YAG laser revived ultra-precisely machined silicon wafers. At certain energy intensities, the laser caused recrystallization, turning the amorphized, dislocated and cracked subsurface layers into the same single-crystal structure as the base material. However, excessive energy input resulted in the formation of tiny particles, suggesting the vaporization and recondensation of silicon [268]. Their efforts also identified critical surface angles at which laser recovery becomes ineffective, providing important guidance for processing curved/sloped surfaces [267]. More recent advances include laser micro-Raman spectroscopy of the laser recovered surface, revealing changes in crystallinity and boron distribution within the laser-treated area, allowing the boron concentration to be adjusted by optimizing laser parameters [173]. Niitsu et al. [175] demonstrated the successful application of this concept, using a nanosecond pulsed Nd:YVO4 laser to recover grinding-induced damage in boron-doped silicon wafers. By fine-tuning the pulse width and peak irradiance, they achieved a remarkably smooth surface with an impressively low roughness of 1 nm *Sa* on curved surfaces of silicon edges and notches, as shown in Fig. 32. This method can be also used for finishing micro lens arrays, grooves, and other micro-structured surfaces of single crystal materials. By controlling the shape, power, incidence angle, and scanning dynamics of the laser beam, laser recovery can be applied to various complex shapes including microscale surface structures. However, due to the small spot size of the laser beam, the SCR of the laser recovery process is very small ($<<1$).

6.4. Electric discharge polishing

Electric discharge polishing (EDP) using a wire electrode, shown in Fig. 33, has emerged in the realm of surface engineering to apply a smooth finish to a variety of materials, from metals to ceramics. In EDP, optimal setting of electrical charge conditions is key to balancing surface roughness, remelting layer thickness, and MRR. As a limitation, EDP can only process electrically conductive materials because it relies on electrical sparks to erode a material.

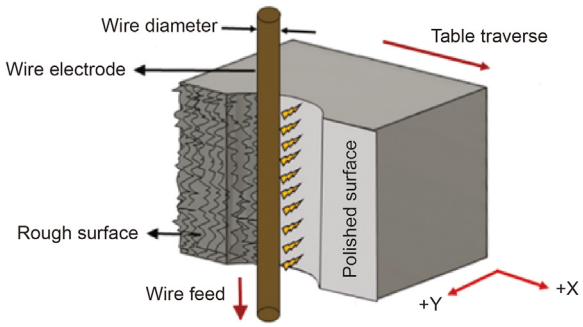

Fig. 33. Schematic of wire EDP finishing of a curved sample [109].

Amorim et al. [8] found that incorporating Mo powder in dielectric fluid and fine-tuning the current increased the hardness of AISI H13 tool steel by a factor of four. Klocke et al. [121] addressed the brittleness of silicon nitride by introducing titanium nitride and explored various methods to minimize the degradation of silicon nitride in EDP. Through analysis and experimentation, Swiercz et al. [226] elucidated the complex interplay of current, pulse duration, and time interval on surface roughness, white layer thickness, and MRR of the tool steel 55NiCrMoV7.

EDP is also finding applications in metal additive manufacturing. In this field, complex parts often have rough surfaces. Hassanin and Boban employed EDP to smoothen Ti-6Al-4V [91] and SS316L [38], achieving impressive roughness reductions. Boban further extended it to AlSi10Mg [36] and TiAl alloys [37], not only refining roughness but also enhancing hardness and corrosion resistance. Jithinraj et al. [109] extended EDP by a geometric model, predicting material removal depth for improved shape accuracy after polishing. In addition, Swiercz et al demonstrated an EDP process that improved the roughness of Ti-6Al-4V by 88% to 0.8 µm *Sa*, revealing an interaction between discharge energy and surface finish [178]. A limitation of wire EDP is the workpiece shape must be able to be tangentially enveloped by the straight wire electrode. The SCR of wire EDP is remarkably higher than that of IBF but still remain very small ($<<1$).

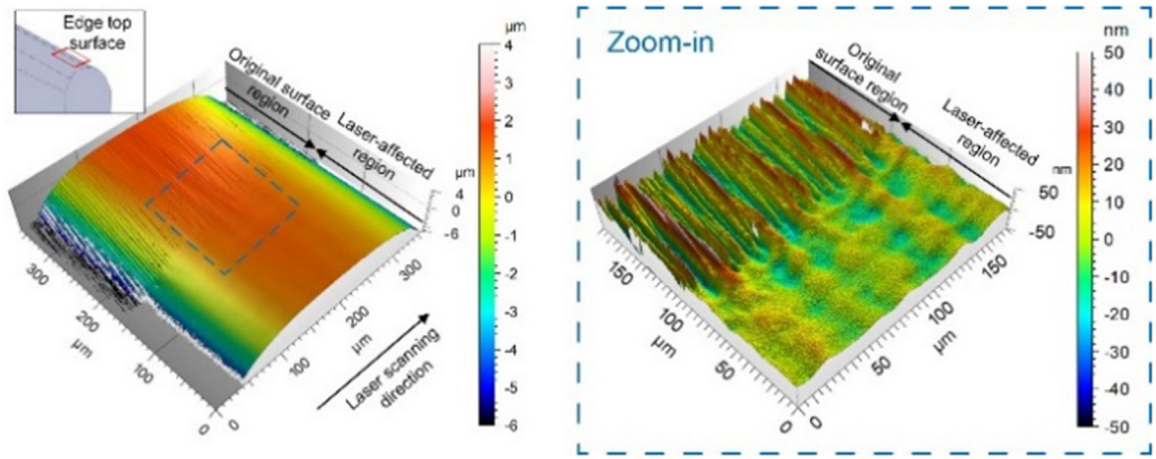

Fig. 32. Three-dimensional surface topography of a silicon wafer edge showing the boundary of original surface and laser-recovered region [174].

7. Processes performance comparison

7.1. Shape adaptability

The evaluation of shape adaptability is of great importance to choose suitable finishing processes to achieve the target with the minimum feature loss and best efficiency and economy. As noted in Section 2, shape adaptability refers to the capability of reducing the surface roughness while simultaneously preserving the intended geometrical features (global and local scale forms) and ensuring minimal MSF generation. The ability of a process to do this depends on the relevant length scales central to the process, tool-surface contact/interaction modes and pose requirements, and general accessibility to the surface in question. Table 2 highlights the attributes and capabilities of the different processing options with respect to form, finish, integrity, and ability to process complex surfaces. Surface finish capabilities are, as always, subject to incoming surface quality, and are dependent on the entire processing chain. Whether an attribute is positive or negative needs to be considered in the context of the desired outcome. For example, chemical solution polishing is highlighted for all 'Complexity' aspects, however uniform processing of local protrusion may be a negative, if said protrusion is a required surface feature. The table does not attempt to comment on either processing efficiencies or material limitations, these are addressed in Sections 7.2 and 7.3 respectively.

7.1.1. Geometric form

Geometric form changes involve two aspects: shape deviation due to the low shape adaptability of the process (negative aspect), and form error correction during finishing (positive aspect). Although form correction is not the central theme of this paper, a subsection of the processes offers the potential to implement form correction in conjunction with the final surface finishing, i.e. processes with smaller SCRs (< 1) and temporally stable material removal based TIFs. Processes with larger SCRs do not offer local material removal discrimination to be employed in this manner, i.e. mass finishing, chemical finishing, etc. The beam-based processes offer the most precision due to their highly repeatable TIFs and smaller projected TIF diameters (sub-millimeter). The tool based loose abrasive processes are routinely engaged in form correction, as are fluid jet polishing and MRF processes.

While the latter portion of Section 2.3 gives an overview of the information required and steps needed to achieve form correction, details within the following papers [27,45,276] give insights into nuances and computational complexity of the process for correcting freeform optics. Even a cursory reading of the literature on this topic will reveal that the success of the entire endeavor centers on the ability to quantify the magnitude of the surface form errors at adequate levels of lateral and vertical resolution. Form measurement approaches include, for example, coordinate measurement machines, optical interferometry, and fringe projection approaches. The complexity of the shape and the acceptable level of deviations strongly influence the ease at which a surface form error map can be generated. For example, the surface form error of the traditional rotationally symmetric spherical or aspherical surfaces mainly manifests in a rotationally symmetric form. Hence, the tolerance analysis of surface deformation for these surfaces are mainly based on radius changes or other equivalent perturbations. Freeform surfaces have no rotational symmetry, and their surface expression is much more complicated. As a result, the fabrication of freeform surfaces is much more complex than the rotational symmetric spherical and aspherical surfaces. And the surface form error of the freeform surfaces cannot be described by a single radius and/or other rotationally symmetric terms [172].

7.1.2. MSF generation

MSF errors occur in processes where the SCR<1 and where the TIF combined with step over distance in the tools programmed path result in locally varied material removal depths or deformation levels at the above-mentioned length scales. While they are inevitable under the conditions listed above, the question to be considered is if they negatively impact the functional performance of the finished surface or not. Typically affected functionalities include optical and cosmetic functionalities. The latter may have no negative mechanical functionality but may be associated with lesser levels of care and craftsmanship thus negatively impact the perceived quality, and consequently value [163]. Within the optical community there is solid literature base describing how MSFs can negatively impact imaging capabilities. The same community has invested in venues for their avoidance though pseudo random paths (Section 2.2) and reduction via fiber based or viscoelastic based tooling (Section 3.1).

As MSFs inherently have associated periodicity, their quantification can be achieved via Fourier transforms and power spectral density analysis [165] of the measured surfaces; these functions are commonly found in commercial dimensional metrology systems. The measured data must have sufficient lateral resolution (at least 2 to

Table 2
Summary table comparing the shape adaptability of different processes.

	Loose abrasive	Fixed abrasive	Stressed finishing	MRF	MAF	Mass finishing	Sand blasting	Fluid jet	Peening	Burnishing	Chemical solution polishing	Dry electro-polishing	Plasma assisted Polishing	Ion beam	Laser	Electron beam
Utilized for form correction	●			●				●						●		
No MSF generation						●					●	●				
Roughness:																
Sa < 10 nm	●			●				●					●	●	●	●
Sa < 0.1 μm		●	●		●	●					●	●				
Sa < 10 μm							●		●	●						
Uniform surface finish expected	●	●		●				●			●	●	●	●	●	●
Integrity																
Removes subsurface damage	●		●	●	●						●	●				
Increases compressive stresses						●	●		●	●						
Complexity																
Tooling with less or no proximity limits						●	●	●	●		●	●		●	●	
Accessibility to re-entrant features					●						●					
Uniform processing of local protrusions											●					
Uniform processing of local gradients								●			●	●	●	●	●	●

5 times finer than the smallest feature) to capture the shorter wavelength periodic features.

7.1.3. Surface roughness

Surface roughness, also called surface texture, is considered the higher frequency content of a surface, i.e. that remaining after form and waviness have been removed from the measurement. The achievable surface finish is determined by process physics and process consumable choices. For example, in loose abrasive processes, the nature of the abrasive (composition, size, shape, etc.), the carrier fluid chemistry and rheological properties, and the pad structure (stiffness, hardness, topography) all influence the final surface roughness. The achievable finishes indicated in Table 2 provide general insights on level of finishes achievable by a process given an optimal set of processing conditions and consumables; specifics for a particular material can vary and will obviously depend on the initial starting state of the surface.

7.1.4. Uniformity of finish

The uniformity of the achievable surface finishes depends on the processes' sensitivity to surface gradients within their individual TIFs and the performance of the tooling over time. In the majority of processes, the produced surface finish within a TIF is expected to be reasonably consistent. The fixed or loose abrasive processes may see variations over time as the tool either holding or entraining the abrasives glazes and alters the removal efficiency. And as outlined in Section 3.2, fixed abrasive processes have regions with differing removal mechanisms and hence different local finishes can be expected. The extent to which this matters depends again on the functionality requirements.

The process requiring most deliberate effort to achieve uniform surface finishes are the mass finishing processes where the orientation of the surfaces within the fluidized abrasive media will strongly impact the contact mode (normal or shear impact) and hence the surface finish outcomes.

7.1.5. Surface integrity

Field and Kahles [72] launched the term surface integrity, which covers the surface and subsurface characteristics (geometrical and metallurgical). Surface and subsurface characteristics including, topography, texture, and material property change, are primary factors that potentially affect the performance and durability of components in various engineering applications. In certain applications, such as optics and semiconductors, subsurface damage needs to be avoided. Abrasive processing and non-mechanical processing, which generate small or zero force, are suitable. However, for other applications, such as bearings and turbine blades, requiring hard and high-resistance surfaces, processing methods that apply significant stress to the workpiece are preferred. Table 2 provides general insights on the surface integrity achievable by each process.

7.1.6. Surface complexity

In the context of freeform surface finishing, four key aspects must be considered in regard to geometrical complexity: accessibility (global gradients), local surface gradients, reentrant features and local protrusions. A key aspect of shape adaptability is the ability of the tooling to have the correct proximity to the workpiece surface to interact with the workpiece under the conditions known to deliver the desired material removal profiles and finishes. In other words, the tooling can access the surface to provide a deterministic TIF. Processes with SCR=1, i.e. those where the workpiece is submerged in the working fluid, obviously have fewer accessibility constraints and thus rank highly in Table 2. Mass finishing while also having a SCR=1, can be access-limited due to the size of its media, with larger media being excluded from smaller, high-slope regions. The beam-based processes, such as laser, ion beam, MRF jet, fluid jet etc., offer reasonable surface accessibility as the beam or jet offer flexibility with respect to the standoff distances between the tool and the workpiece; the tool need not make physical constant with the surface, but it must maintain 'line of sight' with the areas to be processed. The smaller tooling diameters (10s mm to mm in range) also ensure the potential to access a wide range of geometries. Mechanical contact-based processes (fixed and loose abrasive process, MRF, burnishing, etc.) can be most constrained. In this category of processes, the tools must make physical contact with the part under specified orientations to achieve deterministic processing outcomes. If the component's overall surface gradients are great, or highly varying, there just may not be sufficient space for the tooling and its accompanying fixture to get into sufficiently close proximity at with the correct orientation to the surface of interest. Multi axis, high degrees of freedom machine tools with CNC control are needed for surface accessibility. When the correct machine tool, metrology, and machine tool control infrastructure are available, surface gradients can not only be precisely maintained but also corrected with nanometer-level accuracy.

Accommodating surface gradients within a TIFs projected area is most difficult for the mechanical contact-based processes with rigid tooling where the material removal profile is related to the applied pressure profile. TIF-scale local gradients affect the contact areas/pressure distributions and thus the resulting material removal variations. Compliant pads, bonnet-based tools, or even adaptive shape control tools can better accommodate TIF-scale gradients. Reducing the tooling size can also assist in overcoming issues with this category of tools, however this comes at the expense of increased processing time and the risk of imparting MSFs, with shorter length scale MSFs more difficult to remove. For the mechanical non-contact-based processes, and many of the beam-based processes, the material removal rate may remain consistent within a range of standoff distances, in such instances these facilities the preservation of TIF-scale surface gradients. For the chemical and electrochemical processes where the SCR=1, material removal from longer length scale features is typically uniform, however issues will arise when shorter length scale features are present and need to be preserved.

For surface features, such part edges, reentrant feature edges, and corners, some edge and corner rounding will be expected. The extent of rounding depends on how the TIF is affected by the reduced area interacting with the tooling; displacement based mechanical processes will see increased pressures (due to less contact area) thus higher removal rates, force based will be less sensitive to such, but edge roll off can still be expected due to tooling tilt. It's not uncommon for MMR to vary several mm in from the edges. Jet based processes do experience some edge effects. The velocity of the fluid in the edge region can double compared to the inner region, which consequently affects material removal at the ragged edge of the workpiece. Similarly, beam-based processes also face edge effects. For example, laser polishing is generally safe on very blunt edges but problematic on very sharp edges, with higher power levels often causing more edge loss and dulling the sharp edges to some extent.

The fate of protruding surface features will depend on their scale with respect to the process's TIF, with those encompassed within a TIF difficult/impossible to maintain without any loss of geometric fidelity. Masking may help preserve these features to some extent. For example, since polysilicon slurries can be quite selective to oxide and nitride masking films, the polishing process halts once the silicon nitride layer is reached. This allows polysilicon deep trenches to be planarized by CMP [125].

7.2. Processing efficiency

Loose abrasive processes tend to have smaller MRR compared to those with fixed abrasives. A bonnet tool which is an example of the process with loose abrasives exhibits a MRR of 3 mm^3/min in case of polishing BK7. On the other hand, the shape-adaptive grinding with fixed abrasives reaches a MRR of 10 mm^3/min when SiC is processed. The tool radius should be as large as possible under the restriction of the minimum concave radius of the workpiece surface when the maximized efficiency is needed.

Fluid-based abrasive processes have wide variety in terms of the MRR and processing efficiency. An example of the MRR of the mass finishing of aluminum is 2.5 mm^3/min. As stated in Section 3.2.1 the orientation of the workpiece surface relative to dominant media flow direction could affect the MRR. In the case of sand blasting and

abrasive jet machining the MRR is also depending on the impact angle of the abrasives besides other parameters as reported by Ally et al [7]. Nickel based alloy is finished with the MRR of 0.035 mm^3/min by shear stress finishing while it is finished with 0.1 mm^3/min by fluid jet polishing.

Peening is basically a non-material-removal type of process. The efficiency is determined by the surface modification rate instead of the material removal rate. The SCR of shot peening reaches 1200%. The surface roughness can be improved by setting proper SOD and impact angle with the high SCR namely high efficiency [74]. In water jet peening it is important to place workpiece surface with proper SOD against the nozzle. The transition region of the water jet should hit the workpiece surface to enhance the plastic deformation efficiently. In machine hammer peening, the peening head is accelerated toward the workpiece surface pneumatically, electromagnetically and ultrasonically. With the pneumatically driven and electromagnetically driven hammer the oscillating frequency is in the range of several tens to hundreds Hz. With direct sonotrode driven and ultrasonic driven hammer the oscillating frequency could reach several tens of kHz. TIF is as small as that of other peening processes the high oscillating frequency could enhance the efficiency of the surface modification.

Burnishing is another process for surface modification without material removal. Compared to the peening process the burnishing exhibits larger TIF which could contribute to the higher process efficiency. In deep rolling, for example, the rolling speed reaches 50 m/min [13].

Besides mechanical processes, chemical processes are another effective option in terms of processing efficiency. In chemically melting finishing, the workpiece surface is smoothened since the locations with high gradient changes, e.g., due to protrusion [68,145] and sharp corners [227], dissolve faster than other locations. The MRR of 316 steel reaches 30 g/min [17]. The MRR of the same process on Ti–6Al–7Nb alloy is approximately 0.06 g/min [147], while it remains 0.011 g/min for AlSi10Mg [204]. It is noted that the batch process is possible to enhance productivity [52]. In dry electropolishing, material removal is limited to the peaks of the surface, resulting in a high material removal rate. In the case of TiAlN/TiSiN, its thickness can be precisely reduced at a rate of 0.04 μm/min [197]. Dry electropolishing is also applicable to batch processes to improve processing efficiency [80].

Chemomechanical polishing is extensively applied in semi-conductor fabrication. Especially, lots of efforts have been made to achieve a high MRR. For example, silicon carbide is processed with a MRR of 200 nm/h [281]. In another example where sapphire is processed, the MRR is 0.387 μm/h [129]. For flat wafers, batch processing is possible, thus the total production efficiency may be high. For complex shapes, however, batch processing is difficult.

Plasma-assisted polishing is a high-efficiency dry polishing method, achieving a MRR of 2.1 μm/h for diamond [263], 500 nm/h for aluminum nitride [220], and 80 nm/h for silicon carbide [60]. For single-crystal sapphire, the MRR reaches 32 nm/min [19].

Ion beam figuring is applied mainly in optical field and its MRR reaches 1 mm^3/min. Uniformity of material removal can be expected by optimizing the beam scanning paths. In addition, the process is not sensitive to the geometrical gradient of the surface.

Laser polishing is another promising method to finish complex surfaces. Its MRR is, however, negligible compared to conventional polishing processes. Since the main mechanism is thermal melting, only a microscopic layer of material is removed from the top of the workpiece surface via vaporization. Laser peening is similar to laser polishing but no material removal is accompanied. The workpiece surface is modified in a way that the fatigue and corrosion resistance are improved by plastic deformation without significant material removal. Laser recovery is a process for modifying surface/subsurface structures. The process mechanism is dominated by thermal melting and crystallization, therefore the MRR is theoretically zero. The spot size of the laser is usually small ($\sim$20 μm^2) thus the total processing efficiency is highly dependent on the laser scan strategy.

Large-area EB irradiation typically has a beam diameter of $\sim$ 60 mm which covers a large area, enhancing the surface modification rate. As high-energy ions are impinged on the workpiece to remove atoms, the MRR is difficult to precisely quantify. Electrical discharge finishing is a surface finishing process where thermal melting and vaporization are the dominant mechanisms. The MRR ranges from 16 to 22 mm^2/min for finishing Si_3N_4-TiN.

For non-removal processes, however, MRR cannot be defined, which hinders the direct comparison of efficiency of various shape-adaptive finishing processes. Even for the processes with material removal the quantitative comparison of the efficiency is difficult with a single parameter such as MRR. Thus, a novel indicator to compare the processing efficiency of all the processes, normalized processing efficiency (NPE) is introduced here as below:

$$NPE = MRR/V_{\mathrm{Proj}} \tag{5}$$

or

$$NPE = 1/DT \tag{6}$$

where V_{Proj} is the volume supposed to be finally removed in the projected area of the tool on the workpiece surface, DT is the dwell time. NPE can also be interpreted as the inverse of the time of tool-workpiece interaction required to finish the surface at a specific position. For some processes, the workpiece surface is not processed just one time, instead, it may be processed for many times (e.g., peening). In this case, dwell time is the total time of all the tool-workpiece interactions for a specific position on a workpiece.

The comparison of NPE for various processes is summarized in Fig. 34. The material removal and non-removal processes are directly compared. NPE of similar processes which are explained in the same section of this paper tend to have close values of NPE. Although NPE

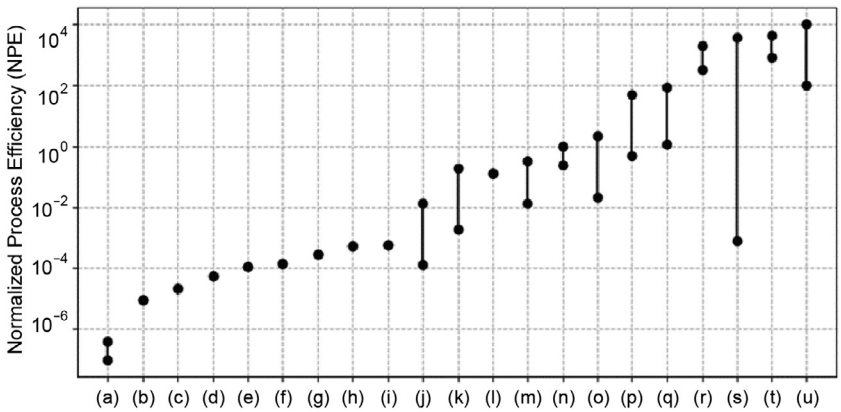

Fig. 34. Comparison of normalized process efficiency for various processes: (a) DEP 316 steels, (b) PAP sapphire, (c) PAP SiC, (d) CMP SiC, (e) CMP sapphire, (f) PAP AlN, (g) DEP copper alloy, (h) SCP 316 steels, (i) PAP diamond, (j) mass finishing, (k) shear stress finishing, (l) fluid jet polishing, (m) sand blasting, (n) IBF, (o) MAF, (p) EB irradiation, (q) EDP, (r) peening, (s) SCP Ti6Al4V, (t) burnishing, (u) laser processes.

does not directly reflect the time needed for the actual processes, NPE multiplied by SCR does. The laser polishing, for example, exhibits a high NPE. However, it normally has a low SCR which makes the process take longer time depending on the workpiece size and laser scan speed.

7.3. Material applicability

Tool-based abrasive processes are applied to various materials such as ceramics, glass and metals. When using industrial robots, the lower stiffness and accuracy of the robot requires the use of adaptive systems for controlling load in the contact area. When the workpiece shows a certain degree of compliance, due to its low rigidity, the process becomes more challenging since the contact conditions are not easy to control. In such cases the estimation of the contact conditions which is fully described by a set of concurrent partial differential equations is needed. Fluid-based abrasive processes are also applicable to various materials. Shear stress finishing, for example, is applied to process optical glass [210], steel alloy SCM435 [171], cemented carbide [47], copper plate [277], nickel-based alloy [211] and steel SKD11 [170].

Mechanical processes without material removal have a wide range of applications to metal materials that exhibit plasticity. The subsurface properties such as residual stress are greatly affected by the parameter in a way that the compressive residual stress has a peak with a certain standoff distance in water jet peening [159]. Another important parameter is the impact angle of the media. For example, the martensitic AISI CA6-NM workpiece exhibited the increase of surface roughness with decreased impact angle in the machine hammer peening. Burnishing is also applied to engineering ceramic [96] and additively manufactured Inconel 718 [264]. When the workpiece with complex geometry is finished, a burnishing tool with spring component is applied for better shape adaptability.

In solution-based chemical processes, the workpiece is limited to the material that exhibits chemical reactions with the solution. Chemical melting finishing is applied to both metal and polymers. The difference between metal dissolution rate and ion diffusion rate makes the workpiece surface smooth eventually. 3D printed polymer such as acrylonitrile butadiene styrene [92] is smoothly finished with the method as well. Chemomechanical polishing is a key technique in semiconductor industries. The chemicals in the slurry lead to a chemically reacted layer on the workpiece such as Si and SiC wafers through chemical oxidation or hydration, which is further removed by mechanical abrasion through the sliding or rolling of abrasives [55]. Plasma-assisted polishing is a highly efficient dry process that is applied to semiconductor materials and metals that show chemical reactions with plasma.

Physical processes are also widely applied to numerous materials. Ion beam figuring is useful for hard brittle or heat-sensitive materials, such as fused silica, silicon, Zerodur, calcium fluoride, copper, SiC, aluminum etc. Laser polishing is applied to hot work steels, titanium alloys, and stainless steel, as well as ceramics, glass and polymers. Laser peening is applied to workpiece materials such as nickel-based alloys, titanium-based alloys, aluminum-based alloys, as well as ceramics and composites. Laser recovery is a unique process applied to single-crystal materials such as silicon. Large-area election beam irradiation is applied to a variety of alloys, such as magnesium alloy, aluminum–silicon alloy, tool steel, and stainless steel.

8. Future Possibilities

As manufacturing demands continue to evolve, advanced surface finishing techniques are becoming increasingly needed, particularly for processing complex geometries and novel materials. In this context, innovative finishing methods are required to address these challenges. Additive manufacturing (AM), for example, present unique challenges due to high roughness, porosity, anisotropic material behavior, and non-uniform geometries. The high potential of shape adaptive processes for post processing of AM parts is expected especially for builds with complex geometry.

As addressed in Sections 3 to 6, significant advances have been demonstrated for surface finishing technologies for complex-shaped workpieces. However, the advances are accompanied by new problems and challenges in the industrial applications of those technologies. To address those problems and challenges, extensive research efforts are required from both the academic and the industrial levels. This requirement means some emerging opportunities for further R&D and breakthroughs in this field.

8.1. Optimal Process Selection

Process selection will always be an optimization challenge bounded by material, final specifications, process availability, costs/time constraints. Selecting the right process for a specific workpiece requires a comprehensive decision-making framework that accounts for material properties, geometry, desired surface quality, processing efficiency, and production cost. Table 2 in Section 7 summarizes some potential selection criteria in terms of achievable surface finish, uniformity and integrity of the generated surfaces. Furthermore, workpiece material characteristics, such as hardness, thermal properties, and surface conditions, influence the prediction of process behavior. The initial workpiece geometry significantly affects process feasibility and efficiency. For industrial applications, suitable systems for processing parts with a wide range of sizes and geometrical features have to be developed. As such, Table 2 aims to provide a useful starting point in process selection and is not intended as a definitive look-up.

For the applicability of the processes discussed in Sections 3 to 6, the accessibility and suitability have to be evaluated considering the mechanical load during finishing of partly filigree components. In this case, plasma-assisted polishing, hybrid processes like electrochemical-mechanical polishing, and laser-assisted mechanical polishing may provide promising solutions by integrating mechanical, chemical, and physical methods. Adaptive tools with compliance for intricate geometries, nano-structured abrasives for ultra-hard materials, and multifunctional designs may enhance the process flexibility and precision. These advancements address diverse material requirements and enable high-quality finishes for ultra-precision applications. It should be pointed out that though some of the processes described in Sections 3 to 6 are commercially available or already used for industrial applications, some others still remain on the laboratory scale and need further development to find industrial applications.

8.2. Modeling and Simulation

As mentioned in Section 2.3, the generation of a TIF dwell time map for each location on the surface is important to achieve form accuracy in the nanometer range which is required in the optical industry. Successfully achieving this requires sufficiently high-resolution height maps of the TIF and current surface form, the ability to create a surface form error map, and appropriate algorithms to both convolve the TIF with the error map to generate the dwell time map and generate the machine code to translate the tooling over the surface at the desired varying speeds to achieve the required local dwell time.

Modelling surface topography evolution as a function of TIF and tool path is another topic of intense discussion and development. Optimizing TIF shapes ensures consistent material removal rates, minimizes defects, and reduces MSF errors. Adaptive TIF generation and real-time feedback systems dynamically adjust parameters like pressure and tool compliance for varying geometries. Predictive models and high-fidelity simulations using tools like finite element analysis (FEA) and computational fluid dynamics (CFD) enable accurate optimization. Novel tool designs, such as elliptical or asymmetrical TIFs, provide specialized solutions for enhanced performance. High-resolution metrology tools integrated with TIF models improve process control and minimize risks of over- or under-polishing.

From the initial proposal for using computers to control sub-aperture polishing processes [45], much literature has been dedicated to

the topic of improving the algorithms used for the computation of convolution (prediction of processed surface topography from a given dwell-time distribution) and deconvolution (retrieval of dwell-time distribution necessary to achieve a target surface topography). The deconvolution problem in particular is severely ill-conditioned. Nevertheless, least-square solutions were found and excellent computability is achievable through the introduction of a damping factor in the iterative computation [46]. More recently, Yamato et al. [265]proposed a novel method that eliminates the need for deconvolution. The concept consists in convoluting the influence function together with a set of spline basis functions used to represent the dwell-time distribution. This creates a set of process basis functions (PBFs) that share the same control points with the dwell basis functions (DBFs). Using the PBFs, the control points are fitted against the target removal profile through conventional spline fitting methodology. Meanwhile, the dwell distribution can be retrieved by applying the control points to the DBFs. This new approach has been shown to provide solutions with a frequency content that overcomes the first zero-power frequency issue observed with traditional least-square methods.

The influence of the tool path layout and its geometric parameters (e.g., track spacing) on the surface generation is an important topic. Projecting a planar raster path onto a freeform surface leads to variable spacing between the tool path tracks, which in turn causes non-uniform material processing for a given dwell-time density. While this can be mitigated through dwell-time moderation, advanced tool path planning strategies for uniform coverage of material removal distribution on freeform surfaces have been proposed [88]. Furthermore, tool paths can be randomized to reduce the occurrence of tool path signature in the power spectral density of the processed surfaces [63].

Besides the need for retrieving the dwell-time distribution, the dynamic capabilities of the machine tool used to deploy the process can also greatly influence the surface generation outcome. In the case of influence functions generated through geometrical contact between a physical tool and the workpiece (e.g., bonnet polishing, shape adaptive grinding, MRF), volumetric errors of the machine may cause large variations of the spot size across the workpiece [142]. More generally, Mizoue et al. [161] have described how the dynamic properties of the control system can create large discrepancies between the actual tool feed profile and intended NC code. The principle is that the intended tool path as specified in the G codes first passes through the control system interpolator where an acceleration filter is applied (e.g., exponential, jerk-limited). Next, the feed drive system introduces further distortion of the signal due to factors such as friction, current limitations, etc. As a result, the actual feed profile may deviate severely from the original G code. When with a raster tool path, this can induce left-to-right and right-to-left shifts between tracks. It has been shown that such issues can be partly mitigated through identification of the control system and modification of the G code [22], but this remains a topic of on-going research. An extensive summary of algorithms and methods for convolution/deconvolution of tool influence functions, as well as the impact of machine and control system dynamics, was featured in the CIRP Novel Topics in Production Engineering [235].

Prediction of the tool influence function as well as the surface coverage ratio depends on the understanding of their relation to the chosen process parameters and the resulting process quantities. A seamless data flow from in-process measurements to a digital representation of the shape adaptive process would, in a first step, allow for establishing digital shadows. Given that the correlations between the process quantities and the resulting surface finish are understood, digital representations controlling the physical representation of shape adaptive processes, i.e., digital twins, can be developed [33,84]. However, achieving this requires not only precise and accurate process evaluation but also high-speed data acquisition. In particular, locally resolved data on process quantities, such as mechanical and thermal loads, provide deeper insights into process behavior, enabling further optimization of both surface quality and overall productivity.

8.3. Surface/subsurface and Process Evaluation

To further clarify the aforementioned process correlations and for a wide implementation of the shape adaptive processes in industrial application, advanced methods for characterization of the key properties of the finished surfaces will be the basis. This may include evaluation methodologies related to surface integrity, particularly focusing on the assessment of shape deviation, feature loss, non-uniformity in surface/subsurface characteristics, as well as the resulting surface functionality of the finished parts. Bayraktar and Pidugu [20] highlighted how microfluidic devices, which gained interest due to their potential applications in various fields including the biomedical industry, face challenges in design due to incomplete understanding of fluid flow in microchannels. The authors emphasized the importance of characterizing liquid flows in microfluidic systems to ensure their effective operation, particularly when feature loss could obstruct fluid flow or alter flow patterns. It is noteworthy that while employing smoothing filters, such as the S-Filter, can be instrumental in noise reduction, they also have the potential to induce shifts in feature boundaries, consequently affecting dimensional characterization outcomes. Convolution-based smoothing filters may inadvertently lead to the attenuation of sharp feature edges, exacerbating the risk of feature loss. To mitigate these challenges, non-linear filters have been developed, with a particular focus on enhancing edge preservation, especially for surfaces characterized by step-like formations, as commonly encountered in MEMS components [105].

For the evaluation of freeform shapes, Galantucci et al. [75] proposed an AI-based approach aligning measured point clouds (3D laser scanner) with the target geometry. The integration of AI in the evaluation and prediction of finished surfaces offers high potential. This is demonstrated in a study using an artificial neural network (ANN) further enhancing the evaluation process by predicting shape-related parameters based on acquired digital images. Additionally, a shadow removal algorithm was introduced to improve image quality, addressing potential distortions caused by inclined surfaces [185].

Berglund et al. [32] introduced an approach for selecting relevant parameters for the evaluation of the post-processing effects, particularly quantifying shape deviation. They presented a novel method that combines conventional areal texture parameters, multiscale analysis, and statistics to achieve a detailed and more relevant surface topography characterization. In this approach, conventional parameters describe types of features, such as peaks, valleys, and texture properties like anisotropy, while area-scale complexity analysis provides information about the size of these features. By using both methods in combination, a more detailed and complete surface texture characterization can be achieved, enabling a better understanding of the observed phenomena. Redford and Mullany [194] proposed a systematic signal detection theory-based framework to assess a metric's ability to differentiate between two different surface classes, or indeed multiple different surfaces. These approaches indicate future developments for advanced characterization of surfaces finished by shape adaptive processes.

Current limitations in evaluation methods such as the linear diffusion filter which is suitable for smooth surfaces but not capable of filtering a structured surface that has sharp edges [106] have furthermore to be addressed in the future. This limitation occurs because linear diffusion is a Gaussian smoothing procedure. For that reason, it does not only reduce noise, but also important features such as edges are smoothed. Limitations are also mentioned by Jiang et al. [106] regarding the morphological filter. Besides this method being time-consuming for large data sets and large structuring elements, the maximum ball radius is limited due to the huge computation involved. In practice, those large radii are often requested, especially for surfaces with forms attached. This can be a driver for further developments and progress within the field of evaluation of finished surfaces.

Leach et al. [127] pointed out the need to overcome various instrumental limitations, one of them being bandwidth limitations of optical instruments. There is a lower wavelength and an upper wavelength limit. Transfer function model limitations were discussed as

well. For rough surfaces, multiple reflections can introduce errors. With multiple reflections occurring, the linear assumptions of the transfer function models are not functioning properly. In the future, a mechanism is needed to calculate the magnitude of the measurement uncertainties caused by the various assumptions, and a calibration technique that applies to rough, strongly scattering surfaces.

Jiang et al. [105] discussed current limitations of cross-correlation methods. First, they cannot easily detect rotational instances. Second, they cannot easily discriminate between salient and less-relevant traits in comparison. A solution to those problems is provided by the polar transform and the Fourier-Mellin transform. Wavelets can be used to isolate individual features as well. The transformation of the topography to other mathematical spaces, for example the Radon transform for linear features and the Ridgelet and Curvelet transforms for curved features also provide solutions. The angular radial transform has been also adapted to operate on height maps and configured to ensure a solution for described limitations.

The shape adaptive processes presented in Sections 3 to 6 have shown to be beneficial for finishing components with a wide range of potential applications. To firmly establish shape adaptive processes in production, the processes must be able to generate finished parts with application-based functionality in terms of customization of surface and subsurface characteristics. Parts finished with the aforementioned shape adaptive processes can show elevated functionality in a medical setting, where surface treatments might prioritize antibacterial properties [199] to mitigate infection risks. In the automotive sector, the focus is different and may be on enhancing scratch resistance to preserve the vehicle's aesthetic appeal over time and realizing stable and better tribological properties [113]. Shape adaptive processes discussed in Section 4 have proven to beneficially modify the finished surface of parts with simple geometries. Building on initial findings in recent work, they can be successfully used for complex parts in the future. To establish shape adaptive processes in the production of parts with functionalities such as water repellence, self-cleaning, anti-icing, and reduction of drag, the processes' impact on the wettability of the surface [50] needs to be quantified and understood. The diversity of functionalities enabled by shape adaptive processes will further extend to include aspects like chemical resistance for industrial applications, optical clarity for display technologies, and biocompatibility for implants and medical devices in the future.

Optical methods [95] will continue to stand as a cornerstone of the evaluation, employing advanced techniques such as optical profilometers, laser scanners and confocal microscopes. White light interferometry [143] further enhances 3D surface topography maps with sub-nanometer resolution, offering a synergistic approach to surface evaluation. Complementary to these are advanced microscopy techniques, including scanning confocal electron microscopy, providing high-resolution imagery that reveals micro and nanoscale surface characteristics. These methods will also in the future be highly relevant because of their precision, accuracy, time aspects and the development of integrating ANN into the evaluation of the optical measurement data. Currently, some attempts have been made. For example, QED Technologies has developed a footprint measurement add-on system for their MRF machines [186]. Zeeko used the Renishaw NC4 on-machine to measure the tool, and 4D NanoCAM to measure the footprint [2].

However, for surfaces with complex shapes finished by shape-adaptive processes, evaluation will remain challenging both in terms of geometrical properties as well as with respect to functionalities such as wear resistance, friction property, reflectivity, or wettability. The technological and quantitative description of complex surfaces that are to fulfil an aesthetic function currently poses a particular challenge.

8.4. Application of Robotics and Artificial Intelligence

Many finishing processes, such as polishing and burnishing, so far depend heavily on human expertise, making them less repeatable and efficient, especially for complex shapes or mass production. Robotics and automation can address these limitations by providing consistent quality and reducing dependence on skilled operators. Advanced robotic systems with multi-axis processing capabilities replicate human adaptability and precision. For example, as demonstrated by Krall et al. [123] in machine hammer peening, the influence of the dynamics and positioning accuracy of the robot have to be fully understood based on comparisons with results from machine tools. Real-time feedback through integrated computer vision systems ensures accurate adjustments during processing. Human-robot collaboration systems balance flexibility and efficiency, with robots performing repetitive tasks while humans oversee decision-making.

Autonomous finishing systems, coupled with simulation-based parameter optimization, further improve productivity and minimize reliance on trial-and-error approaches. Artificial intelligence (AI) and machine learning facilitate automated decision-making and adaptive control, dynamically adjusting parameters such as tool paths and dwell times. Hybrid processes that integrate mechanical and chemical methods provide a balance between performance and cost-effectiveness. To reduce trial-and-error and reliance on human expertise, AI-driven systems are increasingly being used to optimize parameters in real time and enhance efficiency.

AI is also instrumental in determining optimal processing parameters based on workpiece material characteristics. For instance, Iwao et al. [100] demonstrated a machine learning and particle swarm optimization-based system for selecting shape-adaptive grinding parameters. The system processes input data, including material properties such as Young's modulus and hardness, in conjunction with a simplified grain indentation model. This AI-driven approach outperforms human operators in reducing process time while achieving targeted surface conditions. Additionally, AI tools are being used to monitor the evolution of tool influence functions [279], such as changes caused by tool wear.

The integration of AI into surface finishing is revolutionizing process selection, parameter optimization, and decision-making. Machine learning algorithms trained on extensive datasets recommend optimal finishing methods based on material properties and geometry, streamlining workflows and improving efficiency. AI-driven systems dynamically adjust parameters such as pressure and speed to ensure uniform material removal while minimizing defects. Moreover, predictive maintenance systems powered by AI detect wear and misalignment, enabling proactive scheduling and reducing downtime. By integrating AI with computer vision, in-situ surface quality monitoring becomes possible, providing real-time feedback for immediate corrections. Fully automated AI-guided robotic arms further enhance consistency and reduce human intervention. Specialized AI-driven solutions for industries such as optics, aerospace, and biomedical engineering demonstrate the technology's ability to meet stringent industry standards while improving scalability and cost-effectiveness.

9. Conclusions

Surface finishing technology has developed in the past decades where multidisciplinary methodologies have been adopted. However, when these technologies are used for finishing complex surfaces, there are still challenges in terms of shape deviation, feature loss, and surface/subsurface nonuniformity. Hence, shape-adaptive processes are required to reduce surface roughness uniformly while keeping the desired workpiece shape. This keynote paper reviewed and compared major types of shape-adaptive surface finishing processes, including mechanical, chemical, physical processes, from their material removal or redistribution mechanisms, tooling mechanisms, shape adaptability, processing efficiency, and material applicability. This comparison helps identify and select optimal shape-adaptive finishing processes for various complex surfaces to improve the surface quality without losing the form accuracy and surface features. Based on the review and analysis results, the existing problems and challenges, as well as future possibilities and research directions in this emerging field were identified. Further topics for research include process modeling/simulation, digital twin, surface metrology and

functionality evaluation, applications of advanced robotics to the shape-adaptive processes, and integration of AI to process selection, parameter optimization, and process evaluation.

Nomenclature

CMP:	Chemical mechanical polishing	MRR:	Material removal rate
		MSF:	Mid-spatial frequency
DEP:	Dry electropolishing	NPE:	Normalized processing efficiency
EB:	Electron beam		
EDP:	Electric discharge polishing	PAP:	Plasma-assisted polishing
IBF:	Ion beam figuring	SCP:	Solution-based chemical polishing
LSP:	Laser shock peening		
MAF:	Magnetic field assisted finishing	SCR:	Surface coverage ratio
		SOD:	Standoff distance
MRF:	Magnetorheological finishing	SSD:	Subsurface damage
		TIF:	Tool influence function

Declaration of competing interest

The authors declare that they have no known competing financial interests or personal relationships that could have appeared to influence the work reported in this paper.

CRediT authorship contribution statement

Jiwang Yan: Writing – review & editing, Writing – original draft, Visualization, Resources, Project administration, Methodology, Data curation, Conceptualization. **Brigid Mullany:** Writing – review & editing, Writing – original draft, Visualization, Resources, Project administration, Methodology, Data curation, Conceptualization. **Anthony Beaucamp:** Writing – review & editing, Writing – original draft, Visualization, Project administration, Methodology, Data curation, Conceptualization. **Daniel Meyer:** Writing – review & editing, Writing – original draft, Visualization, Resources, Project administration, Methodology, Data curation, Conceptualization. **Naohiko Sugita:** Writing – review & editing, Writing – original draft, Visualization, Resources, Project administration, Methodology, Data curation, Conceptualization.

Acknowledgements

The authors would like to express their sincere thanks to Dr. Toru Kizaki and Dr. Reina Yoshizaki (University of Tokyo), Dr. Lin Zhang (Changchun University of Technology), and Dr. Weihai Huang (Keio University) for their support, contribution and active involvement in the preparation of the manuscript of this paper.

References

[1] Abrão AM, Denkena B, Köhler J, Breidenstein B, Mörke T (2014) The Influence of Deep Rolling on the Surface Integrity of AISI 1060 High Carbon Steel. *Procedia CIRP* 13:31–36.
[2] Ben Achour S, G Bissacco, Beaucamp A, De Chiffre L (2020) Deterministic polishing of micro geometries. *CIRP Annals* 69(1):305–308.
[3] Achtsnick M, Drabbe J, Hoogstrate AM, Karpuschewski B (2004) Erosion behaviour and pattern transfer accuracy of protecting masks for micro-abrasive blasting. *Journal of Materials Processing Technology* 149(1–3):43–49.
[4] Aikens D, Roussel A, Bray M (1995) Derivation of preliminary specifications for transmitted wavefront and surface roughness for large optics used in inertial confinement fusion. *Proceedings of SPIE* 2633:350–360.
[5] Garg Ajay K, Kavanaugh Michael D (1998) *Explosive fragmentation process* .
[6] Allen DM, Shore P, Evans RW, Fanara C, O'Brien W, Marson S, O'Neill W (2009) Ion beam, focused ion beam, and plasma discharge machining. *CIRP Annals* 58 (2):647–662.
[7] Ally S, Spelt JK, Papini M (2012) Prediction of machined surface evolution in the abrasive jet micro-machining of metals. *Wear* 292–293(15):89–99.
[8] Amorim FL, Dalcin VA, Soares P, Mendes LA (2017) Surface modification of tool steel by electrical discharge machining with molybdenum powder mixed in dielectric fluid. *International Journal of Advanced Manufacturing Technology* 91 (1–4):341–350.
[9] Ando M, Negishi M, Takimoto M, Deguchi A, Nakamura N (1995) Super-smooth polishing on aspherical surfaces. *Nanotechnology* 6(4):111.
[10] Andrew Hills M, Scott Malcolm J, Mohamed Dhansay N, Hermann Becker T (2023) High cycle fatigue strength of hot isostatically pressed and chemically etched laser powder bed fusion produced Ti-6Al-4V. *International Journal of Fatigue* 175.
[11] Arnold T, Böhm G, Fechner R, Meister J, Nickel A, Frost F, Hänsel T, Schindler A (2010) Ultra-precision surface finishing by ion beam and plasma jet techniques-status and outlook. *Nuclear Instruments and Methods in Physics Research, Section A: Accelerators, Spectrometers, Detectors and Associated Equipment* 616(2–3):147–156.
[12] Aspden R, McDonough R, Nitchie FR (1972) Computer Assisted Optical Surfacing. *Applied Optics* 11(12):2739–2747.
[13] Bäcker V, Klocke F, Wegner H, Timmer A, Grzhibovskis R, Rjasanow S (2010) Analysis of the deep rolling process on turbine blades using the FEM/BEM-coupling. *IOP Conference Series: Materials Science and Engineering* 10:012134.
[14] Balaji DS, Jeyapoovan T (2021) Optimization of process parameters in water jet peening on Al 6063-T6 alloy using grey relational analysis. *Materials Today: Proceedings* 45:2556–2560.
[15] Balamurugan K, Uthayakumar M, Gowthaman S, Pandurangan R (2018) A study on the compressive residual stress due to waterjet cavitation peening. *Engineering Failure Analysis* 92:268–277.
[16] Barman A, Das M (2017) Design and fabrication of a novel polishing tool for finishing freeform surfaces in magnetic field assisted finishing (MFAF) process. *Precision Engineering* 49:61–68.
[17] Basha MM, Basha SM, Jain VK, Sankar MR (2022) State of the art on chemical and electrochemical based finishing processes for additive manufactured features. *Additive Manufacturing* 58:103028.
[18] Basha SM, Venkaiah N, Srivatsan TS, Sankar MR (2023) Post-processing techniques for metal Additive Manufactured products: role and contribution of abrasive media assisted finishing. *Materials and Manufacturing Processes* 39 (6):737–760.
[19] Bastawros AF, Chandra A, Poosarla PA (2015) Atmospheric pressure plasma enabled polishing of single crystal sapphire. *CIRP Annals* 64(1):515–518.
[20] Bayraktar T, Pidugu SB (2006) Characterization of liquid flows in microfluidic systems. *International Journal of Heat and Mass Transfer* 49(5–6):815–824.
[21] Beaucamp A, Katsuura T, Takata K (2018) Process mechanism in ultrasonic cavitation assisted fluid jet polishing. *CIRP Annals* 67(1):361–364.
[22] Beaucamp A, Mizoue Y, Yamato S, Sencer B (2023) Feed scheduling for time-dependent machining processes by optimization of bulk removal and NC blocks. *Journal of Materials Processing Technology* 312:117786.
[23] Beaucamp A, Namba Y (2013) Super-smooth finishing of diamond turned hard X-ray molding dies by combined fluid jet and bonnet polishing. *CIRP Annals* 62 (1):315–318.
[24] Beaucamp A, Namba Y, Charlton P (2015) Process mechanism in shape adaptive grinding (SAG). *CIRP Annals* 64(1):305–308.
[25] Beaucamp A, Namba Y, Combrinck H, Charlton P, Freeman R (2014) Shape adaptive grinding of CVD silicon carbide. *CIRP Annals* 63(1):317–320.
[26] Beaucamp A, Namba Y, Freeman R (2012) Dynamic multiphase modeling and optimization of fluid jet polishing process. *CIRP Annals* 61(1):315–318.
[27] Beaucamp A, Namba Y, Inasaki I, Combrinck H, Freeman R (2011) Finishing of optical moulds to $\lambda/20$ by automated corrective polishing. *CIRP Annals* 60 (1):375–378.
[28] Beaucamp A, Namba Y, Messelink W, Walker D, Charlton P, Freeman R (2014) Surface integrity of fluid jet polished tungsten carbide. *Procedia CIRP* 13.
[29] Beaucamp A, Simon P, Charlton P, King C, Matsubara A, Wegener K (2017) Brittle-ductile transition in shape adaptive grinding (SAG) of SiC aspheric optics. *International Journal of Machine Tools and Manufacture* 115:29–37.
[30] Beaucamp AT Micro Fluid Jet Polishing. in Yan J, (Ed.) *Micro and Nano Fabrication Technology*, Springer Singapore, Singapore, 1–37.
[31] Beaucamp ATH, Nagai K, Hirayama T, Okada M, Suzuki H, Namba Y (2022) Elucidation of material removal mechanism in float polishing. *Precision Engineering* 73:423–434.
[32] Berglund J, Holmberg J, Wärmefjord K, Söderberg R (2024) Detailed evaluation of topographical effects of Hirtisation post-processing on electron beam powder bed fusion (PBF-EB) manufactured Ti-6Al-4V component. *Precision Engineering* 85(September 2023):319–327.
[33] Bergs T, Biermann D, Erkorkmaz K, M'Saoubi R (2023) Digital twins for cutting processes. *CIRP Annals* 72(2):541–567.
[34] Bleicher F, Lechner C, Habersohn C, Kozeschnik E, Adjassoho B, Kaminski H (2012) Mechanism of surface modification using machine hammer peening technology. *CIRP Annals* 61(1):375–378.
[35] Bleicher F, Lechner C, Habersohn C, Obermair M, Heindl F, Rodriguez Ripoll M (2013) Improving the tribological characteristics of tool and mould surfaces by machine hammer peening. *CIRP Annals* 62(1):239–242.
[36] Boban J, Ahmed A (2022) Electric discharge assisted post-processing performance of high strength-to-weight ratio alloys fabricated using metal additive manufacturing. *CIRP Journal of Manufacturing Science and Technology* 39:159–174.
[37] Boban J, Ahmed A (2023) Finishing the surface micro-layer of additively manufactured TiAl alloy using electro-thermal discharge assisted post-processing. *Journal of Micromanufacturing* 6(2):151–161.
[38] Boban J, Ahmed A, Rahman MA, Rahman M (2020) Wire electrical discharge polishing of additive manufactured metallic components. *Procedia CIRP* 87:321–326.
[39] Boschetto A, Bottini L, Macera L, Veniali F (2020) Post-Processing of Complex SLM Parts by Barrel Finishing. *Applied Sciences* 10(4):1382.
[40] Bouzakis KD, Tsouknidas A, Skordaris G, Bouzakis E, Makrimallakis S, Gerardis S, Katirtzoglou G (2011) Optimization of wet or dry microblasting on PVD films by various Al2O3 grain sizes for improving the coated tools' cutting performance. *Tribology in Industry* 33(2):49–56.
[41] Bouzid S, Bouaouadja N (2000) Effect of impact angle on glass surfaces eroded by sand blasting. *Journal of the European Ceramic Society* 20(4):481–488.
[42] Le Bras C, Rondepierre A, Seddik R, Scius-Bertrand M, Rouchausse Y, Videau L, Fayolle B, Gervais M, Morin L, Valadon S, Ecault R, Furfari D, Berthe L (2019) Laser shock peening: toward the tse of pliable polid polymers for confinement. *Metals* 9(7):1–13.
[43] Brinksmeier E, Garbrecht M, Meyer D (2008) Cold surface hardening. *CIRP Annals* 57(1):541–544.
[44] Brinksmeier E, Karpuschewski B, Yan J, Schönemann L (2020) Manufacturing of multiscale structured surfaces. *CIRP Annals* 69(2):717–739.

[45] Cao Z-C, Cheung CF, Liu MY (2018) Model-based self-optimization method for form correction in the computer controlled bonnet polishing of optical freeform surfaces. *Optics Express* 26(2):2065–2078.
[46] Carnal CL, Egert CM, Hylton KW (1992) Advanced matrix-based algorithm for ion-beam milling of optical components. In: *Proc. SPIE*, 54–62.
[47] Chan J, Koshy P (2020) Tool edge honing using shear jamming abrasive media. *CIRP Annals* 69(1):289–292.
[48] Chaves-Jacob J, Linares JM, Sprauel JM (2015) Control of the contact force in a pre-polishing operation of free-form surfaces realised with a 5-axis CNC machine. *CIRP Annals* 64(1):309–312.
[49] Chen G, Qiao J (2022) Femtosecond-laser-enabled simultaneous figuring and finishing of glass with a subnanometer optical surface. *Optics Letters* 47(15):3860.
[50] Chun DM, Ngo CV, Lee KM (2016) Fast fabrication of superhydrophobic metallic surface using nanosecond laser texturing and low-temperature annealing. *CIRP Annals* 65(1):519–522.
[51] Cook LM (1990) Chemical processes in glass polishing. *Journal of Non-Crystalline Solids* 120(1):152–171.
[52] Crookall JR (1981) Optimizing Batch Manufacture for Multiple Products and Irregular Demand. *CIRP Annals* 30(1):383–387.
[53] Culpan EA, Arrowsmith DJ (1973) The Chemical Polishing of Aluminium. *Transactions of the IMF* 51(1):17–22.
[54] Cvijanovic S, Bordatchev EV, Tutunea-Fatan OR (2023) Applicability of Laser Polishing on Inconel 738 Surfaces Fabricated Through Direct Laser Deposition. *Journal of Laser Micro/Nanoengineering* 18(1):8–14.
[55] Datta D, Rai H, Singh S, Srivastava M, Sharma RK, Gosvami NN (2022) Nanoscale tribological aspects of chemical mechanical polishing: A review. *Applied Surface Science Advances* 11:100286.
[56] DeGroote JE, Marino AE, Wilson JP, Bishop AL, Lambropoulos JC, Jacobs SD (2007) Removal rate model for magnetorheological finishing of glass. *Appl. Opt.* 46 (32):7927–7941.
[57] Deng H, Endo K, Yamamura K (2015) Plasma-assisted polishing of gallium nitride to obtain a pit-free and atomically flat surface. *CIRP Annals* 64(1):531–534.
[58] Deng H, Endo K, Yamamura K (2017) Damage-free finishing of CVD-SiC by a combination of dry plasma etching and plasma-assisted polishing. *International Journal of Machine Tools and Manufacture* 115:38–46.
[59] Deng H, Monna K, Tabata T, Endo K, Yamamura K (2014) Optimization of the plasma oxidation and abrasive polishing processes in plasma-assisted polishing for highly effective planarization of 4H-SiC. *CIRP Annals* 63(1):529–532.
[60] Deng H, Yamamura K (2013) Atomic-scale flattening mechanism of 4H-SiC (0 0 0 1) in plasma assisted polishing. *CIRP Annals* 62(1):575–578.
[61] Denkena B, Kuhlemann P, Breidenstein B, Keitel M, Vogel N (2021) Influence of Turn-Rolling on the Residual Stresses and Microstructure of C45E and the Effects on Fatigue Life under Cyclic Loading. *HTM Journal of Heat Treatment and Materials* 76(3):195–204.
[62] Du C, Dai Y, Guan C, Hu H (2021) High efficiency removal of single point diamond turning marks on aluminum surface by combination of ion beam sputtering and smoothing polishing. *Optics Express* 29(3):3738–3753.
[63] Dunn CR, Walker DD (2008) Pseudo-random tool paths for CNC sub-aperture polishing and other applications. *Optics Express* 16(23):18942.
[64] Eckert S, Vollertsen F (2018) Mechanisms and processing limits of surface finish using laser-thermochemical polishing. *CIRP Annals* 67(1):201–204.
[65] Evans CJ, Paul E, Dornfeld D, Lucca DA, Byrne G, Tricard M, Klocke F, Dambon O, Mullany BA (2003) Material Removal Mechanisms in Lapping and Polishing. *CIRP Annals* 52(2):611–633.
[66] Fähnle OW, Van Brug H, Frankena HJ (1998) Fluid jet polishing of optical surfaces. *Applied Optics* 37(28):6771–6773.
[67] Fang FZ, Zhang XD, Weckenmann A, Zhang GX, Evans C (2013) Manufacturing and measurement of freeform optics. *CIRP Annals* 62(2):823–846.
[68] Fang JL, Han KP (1995) Chemical Polishing of Copper. *Transactions of the IMF* 73 (4):139–141.
[69] Fang Z, Lu L, Chen L, Guan Y (2018) Laser Polishing of Additive Manufactured Superalloy. *Procedia CIRP* 71:150–154.
[70] Fayazfar H, Sharifi J, Keshavarz MK, Ansari M (2023) An overview of surface roughness enhancement of additively manufactured metal parts: a path towards removing the post-print bottleneck for complex geometries. *The International Journal of Advanced Manufacturing Technology* 125(3–4):1061–1113.
[71] Fen Wu J, Lu ZW, Zhang HX, Wang TS (2009) Dwell time algorithm in ion beam figuring. *Applied Optics* 48(20):3930–3937.
[72] Field M, Kahles JF (1964) The surface integrity of machined and ground high-strength steels. *DMIC Report* 210:54–77.
[73] Fleischhauer E, Azimi F, Tkacik P, Keanini R, Mullany B (2016) Application of particle image velocimetry (PIV) to vibrational finishing. *Journal of Materials Processing Technology* 229:322–328.
[74] Fuhr JP, Basha M, Wollmann M, Wagner L (2018) Coverage and Peening Angle Effects in Shot Peening on HCF Performance of Ti-6Al-4V. *Procedia Engineering* 213:682–690.
[75] Galantucci LM, Percoco G, Spina R (2004) An artificial intelligence approach to registration of free-form shapes. *CIRP Annals* 53(1):139–142.
[76] Gao W, Haitjema H, Fang FZ, Leach RK, Cheung CF, Savio E, Linares JM (2019) On-machine and in-process surface metrology for precision manufacturing. *CIRP Annals* 68(2):843–866.
[77] Geng Z, Huang N, Castelli M, Fang F (2023) Polishing Approaches at Atomic and Close-to-Atomic Scale. *Micromachines* 14(2):343.
[78] Ghosh G, Sidpara A, Bandyopadhyay PP (2019) An investigation into the wear mechanism of zirconia-alumina polishing pad under different environments in shape adaptive grinding of WC-Co coating. *Wear* 428–429(15):223–236.
[79] Gisario A, Barletta M, Veniali F (2022) Laser polishing: a review of a constantly growing technology in the surface finishing of components made by additive manufacturing. *International Journal of Advanced Manufacturing Technology* 120 (3–4):1433–1472.
[80] GPAINNOVA DryLyte Technology process.
[81] Guo J, Liu K, Wang Z, Tnay GL (2017) Magnetic field-assisted finishing of a mold insert with curved microstructures for injection molding of microfluidic chips. *Tribology International* 114:306–314.
[82] Guo J, Morita SY, Hara M, Yamagata Y, Higuchi T (2012) Ultra-precision finishing of micro-aspheric mold using a magnetostrictive vibrating polisher. *CIRP Annals* 61(1):371–374.
[83] Guo P, Fang H, Yu J (2006) Edge effect in fluid jet polishing. *Applied Optics* 45 (26):6729–6735.
[84] Guo Y, Klink A, Bartolo P, Guo WG (2023) Digital twins for electro-physical, chemical, and photonic processes. *CIRP Annals* 72(2):593–619.
[85] Han K, Fang J (1998) Study on chemical polishing for stainless steel. *Transactions of the Institute of Metal Finishing* 76(1):24–25.
[86] Han Y, Duan F, Zhu W, Zhang L, Beaucamp A (2020) Analytical and stochastic modeling of surface topography in time-dependent sub-aperture processing. *International Journal of Mechanical Sciences* 175:105575.
[87] Han Y, Liu C, Yu M, Jiang L, Zhu W, Qian L, Beaucamp A (2023) Material removal characteristics in submerged pulsating air jet polishing process. *International Journal of Mechanical Sciences* 257:108534.
[88] Han Y, Zhang L, Guo M, Fan C, Liang F (2018) Tool paths generation strategy for polishing of freeform surface with physically uniform coverage. *The International Journal of Advanced Manufacturing Technology* 95(5):2125–2144.
[89] Harish Shivalingappa D (2020) The influence of ball and roller burnishing process parameters on surface integrity of al 2024 alloy. *Materials Today: Proceedings* 27(2020):1337–1340.
[90] Hashmi AW, Mali HS, Meena A, Saxena KK, Ahmad S, Agrawal MK, Sagbas B, Valerga Puerta AP, Khan MI (2023) A comprehensive review on surface post-treatments for freeform surfaces of bio-implants. *Journal of Materials Research and Technology* 23:4866–4908.
[91] Hassanin H, Modica F, El-Sayed MA, Liu J, Essa K (2016) Manufacturing of Ti–6Al–4V Micro-Implantable Parts Using Hybrid Selective Laser Melting and Micro-Electrical Discharge Machining. *Advanced Engineering Materials* 18 (9):1544–1549.
[92] He Y, Xue G-H, Fu J-Z (2014) Fabrication of low cost soft tissue prostheses with the desktop 3D printer. *Scientific Reports* 4:6973.
[93] Heinzel C, Wagner A (2013) Fine finishing of gears with high shape accuracy. *CIRP Annals* 62(1):359–362.
[94] Hennig W, Feldmann G, Haubold T (2014) Shot peening method for aerofoil treatment of blisk assemblies. *Procedia CIRP* 13:355–358.
[95] Hocken RJ, Chakraborty N, Brown C (2005) Optical Metrology of Surfaces. *CIRP Annals* 54(2):169–183.
[96] Huang W, Tsuchida T, Yan J (2024) Surface morphology formation and subsurface microstructure evolution of zirconia in ultrasonic vibration-assisted burnishing. *Journal of Materials Processing Technology* 333:118586.
[97] Ihara M, Matsubara A, Beaucamp A (2020) Study on removal mechanism at the tool rotational center in bonnet polishing of glass. *Wear* : 454–455.
[98] International Standard (2019) Optics and photonics — Preparation of drawings for optical elements and systems — Part 8: Surface texture. *ISO/DIS 10110-8* .
[99] International Standard (2021) Geometrical product specifications (GPS) — Surface texture: Areal Part 2: Terms, definitions and surface texture parameters. *ISO 25178-2* .
[100] Iwao Y, Beaucamp A (2021) Optimization of polishing process parameters by machine learning. In: *Proceedings of the Japan Society for Precision Engineering Autumn Meeting*, 141–142.
[101] Jacobs SD, Golini D, Hsu Y, Puchebner BE, Strafford D, Prokhorov I V, Fess EM, Pietrowski D, Kordonski WI (1995) Magnetorheological finishing: a deterministic process for optics manufacturing. *Proceedings of SPIE 2576, International Conference on Optical Fabrication and Testing* 2576:372–382.
[102] Jamal M, Morgan M (2017) Design Process Control for Improved Surface Finish of Metal Additive Manufactured Parts of Complex Build Geometry. *Inventions* 2 (4):36.
[103] Jawahir IS, Brinksmeier E, M'Saoubi R, Aspinwall DK, Outeiro JC, Meyer D, Umbrello D, Jayal AD (2011) Surface integrity in material removal processes: Recent advances. *CIRP Annals* 60(2):603–626.
[104] Ji S, Jin M, Zhang X, Zhang L, Zhang Y, Yuan J (2007) Novel gasbag polishing technique for free-form mold. *Jixie Gongcheng Xuebao/Chinese Journal of Mechanical Engineering* 43(8):2–6.
[105] Jiang X, Senin N, Scott PJ, Blateyron F (2021) Feature-based characterisation of surface topography and its application. *CIRP Annals* 70(2):681–702.
[106] Jiang XJ, Whitehouse DJ (2012) Technological shifts in surface metrology. *CIRP Annals* 61(2):815–836.
[107] Jiao C, Li S, Xie X (2009) Algorithm for ion beam figuring of low-gradient mirrors. *Applied Optics* 48(21):4090–4096.
[108] Jing T, Zhang Z-C, Li G-W, Zhao F (2007) A new technology for chemical polishing of copper in weak alkaline solution. *Corrosion Science and Protection Technology* 19(5):367–370.
[109] Jithinraj EK, Ahmed A, Boban J (2022) Improving the surface integrity of additively manufactured curved and inclined metallic surfaces using thermo-electric energy assisted polishing. *Surface and Coatings Technology* 446:128803.
[110] Jones RA (1986) Computer-controlled optical surfacing with orbital tool motion. *Optical Engineering* 25(6):256785.
[111] Ishizawa K, Kurisu H, Yamamoto S, Nomura T, Murashige N (2008) Effect of chemical polishing in titanium materials for low outgassing. *Journal of Physics: Conference Series* 100(9):092023.
[112] Kakinuma Y, Ogawa S, Koto K (2022) Robot polishing control with an active end effector based on macro-micro mechanism and the extended Preston's law. *CIRP Annals* 71(1):341–344.
[113] Kameyama Y, Ohmori H, Kasuga H, Kato T (2015) Fabrication of micro-textured and plateau-processed functional surface by angled fine particle peening followed by precision grinding. *CIRP Annals* 64(1):549–552.

[114] Keanini RG, Tkacik PT, Fleischhauer E, Shahinian H, Sholar J, Azimi F, Mullany B (2017) *Macroscopic liquid-state molecular hydrodynamics*, Nature Publishing Group.
[115] Kersting P, Joliet R, Kansteiner M (2015) Modeling and simulative analysis of the micro-finishing process. *CIRP Annals* 64(1):321–324.
[116] Khany ES, Moyeed MA, Siddiqui MS, Sayeed Ahmed GM, Baig MMA (2015) An Experimental Study of the Effect of Shot Peening on the Low Carbon Steel and Identification of Optimal Process Parameters. *Materials Today: Proceedings* 2 (4–5):3363–3370.
[117] Kim DW, Burge JH (2010) Rigid conformal polishing tool using non-linear viscoelastic effect. *Optics Express* 18(3):2242.
[118] Klocke F, Engelhorn R, Mayer J, Th Weirich (2002) Micro-Analysis of the Contact Zone of Tribologically Loaded Second-Phase Reinforced Sol-Gel-Abrasives. *CIRP Annals* 51(1):245–250.
[119] Klocke F, Klink A, Veselovac D, Aspinwall DK, Soo SL, Schmidt M, Schilp J, Levy G, Kruth JP (2014) Turbomachinery component manufacture by application of electrochemical, electro-physical and photonic processes. *CIRP Annals* 63(2):703–726.
[120] Klocke F, Mader S (2005) Fundamentals of the deep rolling of compressor blades for turbo aircraft engines. *Steel Research International* 76(2–3):229–235.
[121] Klocke F, Olivier M, Degenhardt U, Herrig T, Tombul U (2018) Klink A Investigation on Wire-EDM finishing of titanium nitride doped silicon nitride in CH-based dielectrics. In: *Procedia CIRP*, Elsevier B.V., , 650–653.
[122] Kobayashi T, Sera H, Wakabayashi T, Endo H, Takushima Y, Yan J (2018) Surface Flattening and Nanostructuring of Steel by Picosecond Pulsed Laser Irradiation. *Nanomanufacturing and Metrology* 1(4):217–224.
[123] Krall S, Groza U, Bleicher F (2016) Robot Based Machine Hammer Peening To Generate Defined Surface Structures. *Conference: 13th International Conference on High Speed Machining*, .
[124] Krioni NK, Mingazhev AD, Gafarova VA (2021) Finishing surface treatment of GTE parts with dry electropolishing. *Journal of Physics: Conference Series* 1891 (1):012028.
[125] Landis H, Burke P, Cote W, Hill W, Hoffman C, Kaanta C, Koburger C, Lange W, Leach M, Luce S (1992) Integration of chemical-mechanical polishing into CMOS integrated circuit manufacturing. *Thin Solid Films* 220(1):1–7.
[126] Lazoglu I, Boz Y, Erdim H (2011) Five-axis milling mechanics for complex free form surfaces. *CIRP Annals* 60(1):117–120.
[127] Leach RK, Giusca CL, Haitjema H, Evans C, Jiang X (2015) Calibration and verification of areal surface texture measuring instruments. *CIRP Annals* 64(2):797–813.
[128] Lee D, Lee H, Jeong H (2016) Slurry components in metal chemical mechanical planarization (CMP) process: A review. *International Journal of Precision Engineering and Manufacturing* 17(12):1751–1762.
[129] Lei H, Tong K, Wang Z (2016) Preparation of Ce-doped colloidal SiO2 composite abrasives and their chemical mechanical polishing behavior on sapphire substrates. *Materials Chemistry and Physics* 172:26–31.
[130] Li D, Yang J, Zhao H, Ding H (2022) Contact force plan and control of robotic grinding towards ensuring contour accuracy of curved surfaces. *International Journal of Mechanical Sciences* 227:107449.
[131] Li H, Walker D, Yu G, Sayle A, Messelink W, Evans R, Beaucamp A (2013) Edge control in CNC polishing, paper 2: simulation and validation of tool influence functions on edges. *Optics Express* 21(1):370–381.
[132] Li M, Liu M, Riemer O, Karpuschewski B, Tang C (2021) Origin of material removal mechanism in shear thickening-chemical polishing. *International Journal of Machine Tools and Manufacture* 170:103800.
[133] Li M, Lyu B, Yuan J, Dong C, Dai W (2015) Shear-thickening polishing method. *International Journal of Machine Tools and Manufacture* 94:88–99.
[134] Li X, Fang X, Zhang M, Zhang H, Duan Y, Huang K (2023) Gradient microstructure and prominent performance of wire-arc directed energy deposited magnesium alloy via laser shock peening. *International Journal of Machine Tools and Manufacture* 188:104029.
[135] Li Z, Zou L, Yin J, Huang Y (2020) Investigation of parametric control method and model in abrasive belt grinding of nickel-based superalloy blade. *The International Journal of Advanced Manufacturing Technology* 108(9):3301–3311.
[136] Liao L, Zhang Z, Meng F, Liu D, Liu J, Li Y, Cui X (2021) Novel rotary chemical mechanical polishing on an integral impeller. *Journal of Manufacturing Processes* 66:198–210.
[137] Liborius H, Grund T, Nestler A, Paczkowski G, Schubert A, Lampke T (2021) Influence of the finish-machining by turning and diamond smoothing on the tribological properties of Fe17Cr2Ni0.2C thermally sprayed coatings. *Surface and Coatings Technology* 405:126731.
[138] Lienert F, Gerstenmeyer M, Krall S, Lechner C, Trauth D, Bleicher F, Schulze V (2016) Experimental Study on Comparing Intensities of Burnishing and Machine Hammer Peening Processes. *Procedia CIRP* 45:371–374.
[139] Liu H, Xie L, Lin W, Hong M (2021) Optical Quality Laser Polishing of CVD Diamond by UV Pulsed Laser Irradiation. *Advanced Optical Materials* 9(21):2100537.
[140] Liu J, Li Y, Chen Y, Zhou Y, Wang S, Yuan Z, Jin Z, Liu X (2023) A review of low-temperature plasma-assisted machining: from mechanism to application. *Frontiers of Mechanical Engineering* 18(1):18.
[141] Liu N, Sugimoto K, Yoshitaka N, Yamada H, Sun R, Arima K, Yamamura K (2023) Highly efficient finishing of large-sized single crystal diamond substrates by combining nanosecond pulsed laser trimming and plasma-assisted polishing. *Ceramics International* 49(11):19109–19123.
[142] Liu S, Wang H, Hou J, Zhang Q, Zhong B, Chen X, Zhang M (2022) Morphology characterization of polishing spot and process parameters optimization in magnetorheological finishing. *Journal of Manufacturing Processes* 80:259–272.
[143] Lonardo PM, Trumpold H, De Chiffre L (1996) Progress in 3D Surface Microtopography Characterization. *CIRP Annals* 45(2):589–598.
[144] López De Lacalle LN, Lamikiz A, Muñoa J, Sánchez JA (2005) Quality improvement of ball-end milled sculptured surfaces by ball burnishing. *International Journal of Machine Tools and Manufacture* 45(15):1659–1668.
[145] Lozrt J, Votava J, Henzl R, Kumbár V, Dostál P, Čupera J (2023) Analysis of the Changes in the Mechanical Properties of the 3D Printed Polymer rPET-G with Different Types of Post-Processing Treatments. *Applied Sciences (Switzerland)* 13 (16):9234.
[146] Lunin LS, Sinel'nikov BM, Sysoev IA (2018) Features of Ion-Beam Polishing of the Surface of Sapphire. *Journal of Surface Investigation* 12(5):898–901.
[147] Łyczkowska E, Szymczyk P, Dybała B, Chlebus E (2014) Chemical polishing of scaffolds made of Ti-6Al-7Nb alloy by additive manufacturing. *Archives of Civil and Mechanical Engineering* 14(4):586–594.
[148] Maiss O, Meyer D (2024) Influence of the strain rate on the Surface Integrity on 42CrMo4 generated by machine hammer peening. *Procedia CIRP* 123:499–504.
[149] Manco E, Scherillo F, Guerrera C, Bruno M, El Hassanin A, Franchitti S, Borrelli R, Esposito L (2023) Influence of chemical machining on axial fatigue behaviour of electron beam melted Ti6Al4V parts. *Manufacturing Letters* 35:6–10.
[150] Mannens R, Trauth D, Mattfeld P, Klocke F (2018) Influence of Impact Force, Impact Angle, and Stroke Length in Machine Hammer Peening on the Surface Integrity of the Stainless Steel X3CrNiMo13-4. *Procedia CIRP* 71:166–171.
[151] Marcon A, Melkote SN, Castle J, Sanders DG, Yoda M (2016) Effect of jet velocity in co-flow water cavitation jet peening. *Wear* 360–361:38–50.
[152] Marimuthu S, Triantaphyllou A, Antar M, Wimpenny D, Morton H, Beard M (2015) Laser polishing of selective laser melted components. *International Journal of Machine Tools and Manufacture* 95:97–104.
[153] Martin B, Burge J, Miller S, Smith B, Zehnder R, Zhao C (2006) Manufacture of a 1.7 m prototype of the GMT primary mirror segments. *Frontiers in Optics*, Optica Publishing Group, Rochester, New YorkOFWB3.
[154] Melentiev R, Kang C, Shen G, Fang F (2019) Study on surface roughness generated by micro-blasting on Co-Cr-Mo bio-implant. *Wear* 428–429(December 2018):111–126.
[155] Melia MA, Duran JG, Koepke JR, Saiz DJ, Jared BH, Schindelholz EJ (2020) How build angle and post-processing impact roughness and corrosion of additively manufactured 316L stainless steel. *npj Materials Degradation* 4(1):21.
[156] Meyer D (2012) Cryogenic deep rolling – An energy based approach for enhanced cold surface hardening. *CIRP Annals* 61(1):543–546.
[157] Meyer D, Wielki N (2019) Internal reinforced domains by intermediate deep rolling in additive manufacturing. *CIRP Annals* 68(1).
[158] Min R, Wang L, Cheng Y, Hu X (2021) Dry electrochemical polishing of copper alloy in a medium containing ion-exchange resin. *RSC Adv.* 11 (57):35898–35909.
[159] Ming T, Xue H, Zhang T, Han Y, Peng Q (2022) Improving the corrosion and stress corrosion cracking resistance of 316 L stainless steel in high temperature water by water jet cavitation peening. *Surface and Coatings Technology* 438:128420.
[160] Ming Y, Huang X, Zhou D, Li X (2022) A novel Non-Newtonian fluid polishing technique for zirconia ceramics based on the weak magnetorheological strengthening thickening effect. *Ceramics International* 48(5):7192–7203.
[161] Mizoue Y, Sencer B, Beaucamp A (2020) Identification and optimization of CNC dynamics in time-dependent machining processes and its validation to fluid jet polishing. *International Journal of Machine Tools and Manufacture* 159.
[162] Mohammad AEK, Hong J, Wang D (2018) Design of a force-controlled end-effector with low-inertia effect for robotic polishing using macro-mini robot approach. *Robotics and Computer-Integrated Manufacturing* 49:54–65.
[163] Mullany B, Savio E, Haitjema H, Leach R (2022) The implication and evaluation of geometrical imperfections on manufactured surfaces. *CIRP Annals* 71(2):717–739.
[164] Mullany B, Shahinian H, Navare J, Azimi F, Fleischhauer E, Tkacik P, Keanini R (2017) The application of computational fluid dynamics to vibratory finishing processes. *CIRP Annals* 66(1):309–312.
[165] Muralikrishnan B, Raja J (2009) Surface Finish Parameters II: Autocorrelation, Power Spectral Density, Bearing Area. in Muralikrishnan B, Raja J, (Eds.) *Computational Surface and Roundness Metrology*, Springer London, London, 191–199.
[166] Murashova NM, Levchishin SY, Subcheva EN, Krasnova OG, Yurtov EV (2020) Chemical Polishing of Aluminum Using Acid-Containing Reverse Microemulsions. *Protection of Metals and Physical Chemistry of Surfaces* 56(3):560–566.
[167] Murray JW, Clare AT (2012) Repair of EDM induced surface cracks by pulsed electron beam irradiation. *Journal of Materials Processing Technology* 212 (12):2642–2651.
[168] Murray JW, Kinnell PK, Cannon AH, Bailey B, Clare AT (2013) Surface finishing of intricate metal mould structures by large-area electron beam irradiation. *Precision Engineering* 37(2):443–450.
[169] Negi VS, Wang T, Garg H, Pullen WC, Ke X, Kumar RR S, Choi H, Tiwari UK, Karar V, Kim D (2022) Random adaptive tool path for zonal optics fabrication. *Optics Express* 30(16):29295.
[170] Nguyen D (2020) Simulation and experimental study on polishing of spherical steel by non-Newtonian fluids. *International Journal of Advanced Manufacturing Technology* 107(1–2):763–773.
[171] Nguyen DN, Dao TP, Prakash C, Singh S, Pramanik A, Krolczyk G, Pruncu CI (2020) Machining parameter optimization in shear thickening polishing of gear surfaces. *Journal of Materials Research and Technology* 9(3):5112–5126.
[172] Ni J, Yang T, Liu Y, Cheng D, Wang Y (2019) Description and tolerance analysis of freeform surface figure error using specific-probability-distributed Gaussian radial basis functions. *Optics Express* 27(22):31820–31839.
[173] Niitsu K, Tayama Y, Kato T, Maehara H, Yan J (2018) Characterization of recrystallized depth and dopant distribution in laser recovery of grinding damage in single-crystal silicon. *Materials Science in Semiconductor Processing* 82:54–61.
[174] Niitsu K, Tayama Y, Kato T, Yan J (2019) Laser recovery of grinding-induced subsurface damage in the edge and notch of a single-crystal silicon wafer. *Surface Topography: Metrology and Properties* 7(1).
[175] Niitsu K, Yan J (2020) Effects of deep subsurface damages on surface nanostructure formation in laser recovery of grinded single-crystal silicon wafers. *Precision Engineering* 62:213–222.

[176] Okada A, Uno Y, McGeough JA, Fujiwara K, Doi K, Uemura K, Sano S (2008) Surface finishing of stainless steels for orthopedic surgical tools by large-area electron beam irradiation. *CIRP Annals* 57(1):223–226.

[177] Okada A, Uno Y, Yabushita N, Uemura K, Raharjo P (2004) High efficient surface finishing of bio-titanium alloy by large-area electron beam irradiation. *Journal of Materials Processing Technology* 149(1–3):506–511.

[178] Oniszczuk-Świercz D, Świercz R (2023) Effects of Wire Electrical Discharge Finishing Cuts on the Surface Integrity of Additively Manufactured Ti6Al4V Alloy. *Materials* 16(15).

[179] Oranli E, Gungoren N, Heydari Astaraee A, Maleki E, Bagherifard S, Guagliano M (2023) Numerical and experimental analysis of sand blasting on polymeric substrates. *Forces in Mechanics* 12(June):100208.

[180] Pan X, Zhou L, Wang C, Yu K, Zhu Y, Yi M, Wang L, Wen S, He W, Liang X (2023) Microstructure and residual stress modulation of 7075 aluminum alloy for improving fatigue performance by laser shock peening. *International Journal of Machine Tools and Manufacture* 184.

[181] Perenda J, Trajkovski J, Žerovnik A, Prebil I (2015) Residual stresses after deep rolling of a torsion bar made from high strength steel. *Journal of Materials Processing Technology* 218:89–98.

[182] Peyre P, Fabbro R, Merrien P, Lieurade HP (1996) Laser shock processing of aluminium alloys. Application to high cycle fatigue behaviour. *Materials Science and Engineering: A* 210(1–2):102–113.

[183] Pfefferkorn FE, Duffie NA, Li X, Vadali M, Ma C (2013) Improving surface finish in pulsed laser micro polishing using thermocapillary flow. *CIRP Annals* 62(1):203–206.

[184] Pratap A, Yamato S, Beaucamp A (2023) Hybrid tool combining stiff and elastic grinding. *CIRP Annals* .

[185] Priya P, Ramamoorthy B (2007) The influence of component inclination on surface finish evaluation using digital image processing. *International Journal of Machine Tools and Manufacture* 47(3–4):570–579.

[186] QED Technologies https://qedmrf.com/mrf-polishing/qds-deflectometer/.

[187] Qian W, Cai J, Xin Z, Ye Y, Dai F, Hua Y (2022) Femtosecond laser polishing with high pulse frequency for improving performance of specialised aerospace material systems: MCrAlY coatings in thermal barrier coating system. *International Journal of Machine Tools and Manufacture* 182.

[188] Qin M, Ju DY, Oba R (2006) Investigation of the influence of incidence angle on the process capability of water cavitation peening. *Surface and Coatings Technology* 201(3–4):1409–1413.

[189] Rajput AS, Das M, Kapil S (2022) Investigations on a hybrid chemo-magneto-rheological finishing process for freeform surface quality enhancement. *Journal of Manufacturing Processes* 81:522–536.

[190] Ramsden JJ, Allen DM, Stephenson DJ, Alcock JR, Peggs GN, Fuller G, Goch G (2007) The Design and Manufacture of Biomedical Surfaces. *CIRP Annals* 56 (2):687–711.

[191] Rausch S, Wiederkehr P, Biermann D, Zabel A, Selvadurai U, Hagen L, Tillmann W (2016) Influence of Machine Hammer Peening on the Tribological Behavior and the Residual Stresses of Wear Resistant Thermally Sprayed Coatings. *Procedia CIRP* 45:275–278.

[192] Rautio T, Jaskari M, Hietala M, Järvenpää A (2022) Comparison of Polishing Methods: The Effect on The Surface Roughness and Fatigue Performance of PBF-LB manufactured 316L Stainless Steel. *2022 7th National Scientific Conference on Applying New Technology in Green Buildings (ATiGB)*, 51–55.

[193] Rautio T, Jaskari M, Päkkilä J, Järvenpää A (2023) Dry Electropolishing of Laser Powder Bed Fusion Manufactured Cobalt-chrome. *IOP Conference Series: Materials Science and Engineering* 1280(1):012014.

[194] Redford J, Mullany B (2023) Construction of a multi-class discrimination matrix and systematic selection of areal texture parameters for quantitative surface and defect classification. *Journal of Manufacturing Systems* 71:131–143.

[195] Ren X, Cabaravdic M, Zhang X, Kuhlenkötter B (2007) A local process model for simulation of robotic belt grinding. *International Journal of Machine Tools and Manufacture* 47(6):962–970.

[196] Riu G, Weil D, Llanes L, Johanns KE, Oliver WC, Roa JJ (2022) Surface integrity of new dry-electropolishing technology on WC-Co cemented carbides. *Procedia CIRP* 108:543–548.

[197] Riu-Perdrix G, Azkona I, Llanes L, Roa JJ (2024) Stripping process of TiAlN/TiSiN coating on WC-Co cemented carbide substrate by using the dry-electropolishing technique. *Surface and Coatings Technology* 489:131045.

[198] Rolland JP, Davies MA, Suleski TJ, Evans C, Bauer A, Lambropoulos JC, Falaggis K (2021) Freeform optics for imaging. *Optica* 8(2):161.

[199] Romoli L, Lazzini G, Lutey AHA, Fuso F (2020) Influence of ns laser texturing of AISI 316L surfaces for reducing bacterial adhesion. *CIRP Annals* 69(1):529–532.

[200] Rosa B, Mognol P, Hascoët J (2015) Laser polishing of additive laser manufacturing surfaces. *Journal of Laser Applications* 27(S2).

[201] Rotella G, Filice L, Micari F (2020) Improving surface integrity of additively manufactured GP1 stainless steel by roller burnishing. *CIRP Annals* 69(1):513–516.

[202] Sanders D, Soyama H, De Silva C (2021) Use of Cavitation Abrasive Surface Finishing to Improve the Fatigue Properties of Additive Manufactured Titanium Alloy Ti6Al4V. *SAE Technical Papers* . (2021).

[203] Schäfer M, L'huillier JA (2020) Ultrashort-pulse laser micro-polishing of lithium niobate by using UV-ps pulses. In: *Proceedings of SPIE 11268, Laser-based Micro- and Nanoprocessing XIV; 112680R*, .

[204] Scherillo F (2019) Chemical surface finishing of AlSi10Mg components made by additive manufacturing. *Manufacturing Letters* 19:5–9.

[205] Schindler A, Haensel T, Flamm D, Frank W, Boehm G, Frost F, Fechner R, Bigl F (2001) Rauschenbach B Ion beam and plasma jet etching for optical component fabrication. In: *Proceedings of SPIE 4440, International Symposium on Optical Science and Technology*, 217–227.

[206] Schmidt M, Merklein M, Bourell D, Dimitrov D, Hausotte T, Wegener K, Overmeyer L, Vollertsen F, Levy GN (2017) Laser based additive manufacturing in industry and academia. *CIRP Annals* 66(2):561–583.

[207] Schulze V, Bleicher F, Groche P, Guo YB, Pyun YS (2016) Surface modification by machine hammer peening and burnishing. *CIRP Annals* 65(2):809–832.

[208] Shahinian H, Cherukuri H, Mullany B (2016) Evaluation of fiber-based tools for glass polishing using experimental and computational approaches. *Applied Optics* 55(16).

[209] Shahinian H, Hassan M, Cherukuri H, Mullany BA (2017) Fiber-based tools: material removal and mid-spatial frequency error reduction. *Applied Optics* 56 (29):8266.

[210] Shao Q, Duan S, Fu L, Lyu B, Zhao P, Yuan J (2021) Shear thickening polishing of quartz glass. *Micromachines* 12(8).

[211] Shao Q, Lyu B, Yuan J, Wang X, Ke M, Zhao P (2021) Shear thickening polishing of the concave surface of high-temperature nickel-based alloy turbine blade. *Journal of Materials Research and Technology* 11:72–84.

[212] Shiganov I, Melnikov D, Misyurov A, Melnikova M, Shtereveria D, Myat Z (2020) Investigation the effect of laser ablation parameters in a liquid in order to reduce the pulse energy during laser shock peening. *Optical and Quantum Electronics* 52 (4):1–13.

[213] Shinonaga T, Yamaguchi A, Okamoto Y, Okada A (2021) Surface smoothing and repairing of additively manufactured metal products by large-area electron beam irradiation. *CIRP Annals* 70(1):143–146.

[214] Singh RK, Lee S-M, Choi K-S, Bahar Basim G, Choi W, Chen Z, Moudgil BM (2002) Fundamentals of Slurry Design for CMP of Metal and Dielectric Materials. *MRS Bulletin* 27(10):752–760.

[215] Soyama H, Iga Y (2023) Laser Cavitation Peening: A Review. *Applied Sciences (Switzerland)* 13(11).

[216] Soyama H, Korsunsky AM (2022) A critical comparative review of cavitation peening and other surface peening methods. *Journal of Materials Processing Technology* 305:117586.

[217] Span J, Koshy P, Klocke F, Müller S, Coelho R (2017) Dynamic jamming in dense suspensions: Surface finishing and edge honing applications. *CIRP Annals* 66 (1):321–324.

[218] Srivastava M, Tripathi R, Hloch S, Chattopadhyaya S, Dixit AR (2016) Potential of Using Water Jet Peening as a Surface Treatment Process for Welded Joints. *Procedia Engineering* 149:472–480.

[219] Sun R, Nozoe A, Nagahashi J, Arima K, Kawai K, Yamamura K (2021) Novel highly-efficient and dress-free polishing technique with plasma-assisted surface modification and dressing. *Precision Engineering* 72:224–236.

[220] Sun R, Yang X, Arima K, Kawai K, Yamamura K (2020) High-quality plasma-assisted polishing of aluminum nitride ceramic. *CIRP Annals* 69(1):301–304.

[221] Sundar R, Ganesh P, Gupta RK, Ragvendra G, Pant BK, Kain V, Ranganathan K, Kaul R, Bindra KS (2019) Laser Shock Peening and its Applications: A Review. *Lasers in Manufacturing and Materials Processing* 6(4):424–463.

[222] Suratwala T, Menapace J, Steele R, Wong L, Tham G, Ray N, Bauman B, Gregory M, Hordin T (2021) Mechanisms influencing and prediction of tool influence function spots during hemispherical sub-aperture tool polishing on fused silica. *Applied Optics* 60(1):201.

[223] Suzuki H, Hamada S, Okino T, Kondo M, Yamagata Y, Higuchi T (2010) Ultraprecision finishing of micro-aspheric surface by ultrasonic two-axis vibration assisted polishing. *CIRP Annals* 59(1):347–350.

[224] Suzuki H, Kodera S, Hara S, Matsunaga H, Kurobe T (1989) Magnetic field-assisted polishing - application to a curved surface. *Precision Engineering* 11 (4):197–202.

[225] Suzuki H, Okada M, Lin W, Morita S, Yamagata Y, Hanada H, Araki H, Kashima S (2014) Fine finishing of ground DOE lens of synthetic silica by magnetic field-assisted polishing. *CIRP Annals* 63(1):313–316.

[226] Świercz R, Oniszczuk-Świercz D, Chmielewski T (2019) Multi-response optimization of electrical discharge machining using the desirability function. *Micromachines* 10(1).

[227] Takagishi K, Umezu S (2017) Development of the Improving Process for the 3D Printed Structure. *Scientific Reports* 7.

[228] Takizawa K, Beaucamp A (2017) Comparison of tool feed influence in CNC polishing between a novel circular-random path and other pseudo-random paths. *Optics Express* 25(19):22411.

[229] Tang J, Zhang Y, Li X, Wang Q, Zhou P, Zhang L, He Q, Deng H (2024) Conformal polishing of a glass microlens array through oxyhydrogen flame-induced viscoelasticity flow at nano/microscale. *Journal of Materials Processing Technology* 328:118420.

[230] Tani G, Orazi L, Fortunato A, Ascari A, Campana G (2011) Warm Laser Shock Peening: New developments and process optimization. *CIRP Annals* 60(1):219–222.

[231] Taylor LL, Xu J, Pomerantz M, Smith TR, Lambropoulos JC, Qiao J (2019) Femtosecond laser polishing of germanium [Invited]. *Optical Materials Express* 9 (11):4165.

[232] Temmler A, Liu D, Preußner J, Oeser S, Luo J, Poprawe R, Schleifenbaum JH (2020) Influence of laser polishing on surface roughness and microstructural properties of the remelted surface boundary layer of tool steel H11. *Materials and Design* 192:108689.

[233] Temmler A, Willenborg E, Wissenbach K (2012) Laser Polishing. *Laser Applications in Microelectronic and Optoelectronic Manufacturing (LAMOM) XVII* 8243:82430W.

[234] Tokunaga J, Kojima T, Kinuta S, Wakabayashi K, Nakamura T, Yatani H, Sohmura T (2009) Large-area electron beam irradiation for surface polishing of cast titanium. *Dental Materials Journal* 28(5):571–577.

[235] Tolio T, (Ed.) *CIRP Novel Topics in Production Engineering: Volume 1*, Springer Nature Switzerland, Cham.

[236] Tönshoff HK, Kroos F, Marzenell C (1997) High-Pressure Water Peening-a New Mechanical Surface-Strengthening Process. *CIRP Annals* 46(1):113–116.

[237] Tosello G, Bissacco G, Cao J, Axinte D (2023) Modeling and simulation of surface generation in manufacturing. *CIRP Annals* 72(2):753–779.

[238] Tsegaw AA, Shiou F-J, Lin S-P (2015) Ultra-precision polishing of N-Bk7 using an innovative self-propelled abrasive fluid multi-jet polishing tool. *Machining Science and Technology* 19(2):262–285.

[239] Tsuchida T, Huang W, Yan J (2023) Surface conditioning of zirconia ceramic by enhanced ultrasonic vibration-assisted burnishing. *Production Engineering* 18:353–366.

[240] Tyagi P, Goulet T, Riso C, Stephenson R, Chuenprateep N, Schlitzer J, Benton C, Garcia-Moreno F (2019) Reducing the roughness of internal surface of an additive manufacturing produced 316 steel component by chempolishing and electropolishing. *Additive Manufacturing* 25:32–38.

[241] Uhlmann E, Eulitz A, Dethlefs A (2015) Discrete Element Modelling of Drag Finishing. *Procedia CIRP* 31:369–374.

[242] Uno Y, Okada A, Uemura K, Raharjo P, Furukawa T, Karato K (2005) High-efficiency finishing process for metal mold by large-area electron beam irradiation. *Precision Engineering* 29(4):449–455.

[243] Uno Y, Okada A, Uemura K, Raharjo P, Sano S, Yu Z, Mishima S (2007) A new polishing method of metal mold with large-area electron beam irradiation. *Journal of Materials Processing Technology* 187−188(12):77–80.

[244] Vahdati M, Rasouli SA (2016) Study of magnetic abrasive finishing on freeform surface. *Transactions of the Institute of Metal Finishing* 94(6):294–302.

[245] Walker DD, Freeman R, Morton R, McCavana G, Beaucamp A (2006) Use of the 'Precessions'^{TM} process for prepolishing and correcting 2D & $2^{1}/_{2}$D form. *Optics Express* 14(24).

[246] Wan L, Zou Y, Shi S, Tao W, Ju Y (2021) Surface finishing method based on laser re-melting using a cone annular beam for additive manufacturing. *Optics Express* 29(25):42287–42305.

[247] Wang C, Cheung CF, Ho LT, Yung KL, Kong L (2020) A novel magnetic field-assisted mass polishing of freeform surfaces. *Journal of Materials Processing Technology* 279:116552.

[248] Wang D, Shinmura T, Yamaguchi H (2004) Study of magnetic field assisted mechanochemical polishing process for inner surface of Si3N4 ceramic components finishing characteristics under wet finishing using distilled water. *International Journal of Machine Tools and Manufacture* 44(14):1547–1553.

[249] Wang K, Li W, Qu Q, Wang Z (2020) Chemical mechanical polishing of the narrow channel of a channel-cut crystal. *International Journal of Advanced Manufacturing Technology* 108(5−6):1691–1700.

[250] Wang S, Timsit RS, Spelt JK (2000) Experimental investigation of vibratory finishing of aluminum. *Wear* 243(1−2):147–156.

[251] Wang Y, Wu Y, Mitsuyoshi N (2016) A novel magnetic field-assisted polishing method using magnetic compound slurry and its performance in mirror surface finishing of miniature V-grooves. *AIP Advances* 6(5):056602.

[252] Wang Y, Yang J, Li D, Ding H (2021) Tool path generation with global interference avoidance for the robotic polishing of blisks. *The International Journal of Advanced Manufacturing Technology* 117(3−4):1223–1232.

[253] Wang Z, Wu L, Fang Y, Dun A, Zhao J, Xu X, Zhu X (2022) Application of Flow Field Analysis in Ion Beam Figuring for Ultra-Smooth Machining of Monocrystalline Silicon Mirror. *Micromachines* 13(2):318.

[254] West SC, Martin HM, Nagel RH, Young RS, Davison WB, Trebisky TJ, DeRigne ST, Hille BB (1994) Practical design and performance of the stressed-lap polishing tool. *Applied Optics* 33(34):8094.

[255] Wied J *Oberflächenbehandlung von Umformwerkzeugen durch Festklopfen*. 2011.

[256] Wong L, Gregory M, Ray N, Suratwala T, Menapace J, Bauman B, Hordin T, Steele R, Tham G (2021) Effect of workpiece curvature on the tool influence function during hemispherical sub-aperture tool glass polishing. *Applied Optics* 60(4):1041–1050.

[257] Woo H-G, Kim J-S, Ryu J-Y, Lee J-S, Lee S-J (2020) Dry Electropolishing of an Additively Manufactured Spacer Grid. *Transactions of the Korean Nuclear Society Virtual Spring Meeting*, .

[258] Yabuki A, Baghbanan MR, Spelt JK (2002) Contact forces and mechanisms in a vibratory finisher. *Wear* 252(7−8):635–643.

[259] Yamaguchi H, Graziano AA (2014) Surface finishing of cobalt chromium alloy femoral knee components. *CIRP Annals* 63(1):309–312.

[260] Yamaguchi H, Kang J, Hashimoto F (2011) Metastable austenitic stainless steel tool for magnetic abrasive finishing. *CIRP Annals* 60(1):339–342.

[261] Yamaguchi H, Li M, Hanada K (2019) Surface finishing of biodegradable stents. *CIRP Annals* 68(1):357–360.

[262] Yamaguchi H, Nteziyaremye V, Stein M, Li W (2015) Hybrid tool with both fixed-abrasive and loose-abrasive phases. *CIRP Annals* 64(1):337–340.

[263] Yamamura K, Emori K, Sun R, Ohkubo Y, Endo K, Yamada H, Chayahara A, Mokuno Y (2018) Damage-free highly efficient polishing of single-crystal diamond wafer by plasma-assisted polishing. *CIRP Annals* 67(1):353–356.

[264] Yaman N, Sunay N, Kaya M, Kaynak Y (2022) Enhancing Surface Integrity of Additively Manufactured Inconel 718 by Roller Burnishing Process. *Procedia CIRP* 108:681–686.

[265] Yamato S, Sencer B, Beaucamp A (2024) Concurrent process and feedrate scheduling with convoluted basis functions and its application to fluid jet polishing. *International Journal of Machine Tools and Manufacture* 197:104135.

[266] Yan J, Asami T, Kuriyagawa T (2007) Response of machining-damaged single-crystalline silicon wafers to nanosecond pulsed laser irradiation. *Semiconductor Science and Technology* 22(4):392–395.

[267] Yan J, Kobayashi F (2013) Laser recovery of machining damage under curved silicon surface. *CIRP Annals* 62(1):199–202.

[268] Yan J, Sakai S, Isogai H, Izunome K (2009) Recovery of microstructure and surface topography of grinding-damaged silicon wafers by nanosecond-pulsed laser irradiation. *Semiconductor Science and Technology* 24(10):105018.

[269] Yang D-H, Kim Y-K, Hwang Y, Kim M-S, Lee K-A (2019) Effect of Dry-Electropolishing on the High Cycle Fatigue Properties of Ti-6Al-4V Alloy Manufactured by Selective Laser Melting. *Journal of Powder Materials* 26(6):471–476.

[270] Yang J, Chen H, Qi R, Ding H, Yin Y (2023) A novel approach to robotic grinding guaranteeing profile accuracy using rigid-flexible coupling force control for free-formed surfaces. *CIRP Annals* 72(1):313–316.

[271] Yin L, Da Y, Hu H, Guan C (2023) Fluid lubricated polishing based on shear thickening. *Optics Express* 31(1):698.

[272] Yung KC, Xiao TY, Choy HS, Wang WJ, Cai ZX (2018) Laser polishing of additive manufactured CoCr alloy components with complex surface geometry. *Journal of Materials Processing Technology* 262:53–64.

[273] Zeuner M, Kiontke S (2012) Ion Beam Figuring Technology in Optics Manufacturing. *Optik & Photonik* 7(2):56–58.

[274] Zhang D, Zhang XM, Ding H (2020) Experimental and numerical study of the subsurface deformation and residual stress during the roller burnishing process. *Procedia CIRP* 87(March):491–496.

[275] Zhang J, Yao C, Tan L, Cui M, Lin Z, Han W, Min X (2021) Shot peening parameters optimization based on residual stress-induced deformation of large fan blades. *Thin-Walled Structures* 161:107467.

[276] Zhang L, Huang D, Zhou W, Fan C, Ji S, Zhao J (2017) Corrective polishing of freeform optical surfaces in an off-axis three-mirror imaging system. *The International Journal of Advanced Manufacturing Technology* 88(9):2861–2869.

[277] Zhang M, Zhang P, Yang Z, Guo J (2022) A new method for V-groove microstructured surface polishing using non-Newtonian fluids. In: *Proc. of the 9th Intl. Conf. of Asian Society for Precision Engg. and Nanotechnology*, .

[278] Zhang X, Liu J, Xia M, Hu Y (2023) Laser shock peening enables 3D gradient metal structures: A case study on manufacturing self-armored hydrophobic surfaces. *International Journal of Machine Tools and Manufacture* : 185.

[279] Zhang Y, Xiao G, Ma J, Gao H, Zhu B, Huang Y (2024) A hybrid approach of process reasoning and artificial intelligence-based intelligent decision system framework for fatigue life of belt grinding. *The International Journal of Advanced Manufacturing Technology* 130(1):311–328.

[280] Zhao L, Cheng J, Chen M, Yuan X, Liao W, Liu Q, Yang H, Wang H (2019) Formation mechanism of a smooth, defect-free surface of fused silica optics using rapid CO2 laser polishing. *International Journal of Extreme Manufacturing* 1(3):035001.

[281] Zhou Y, Pan G, Zou C, Wang L (2017) Chemical Mechanical Polishing (CMP) of SiC Wafer Using Photo-Catalyst Incorporated Pad. *ECS Journal of Solid State Science and Technology* 6(9):P603.

[282] Zhu W-L, Beaucamp A (2019) Zernike mapping of optimum dwell time in deterministic fabrication of freeform optics. *Optics Express* 27(20):28692.

[283] Zhu W-L, Beaucamp A (2020) Investigation of critical material removal transitions in compliant machining of brittle ceramics. *Materials and Design* 185:108258.

[284] Zhu W-L, Beaucamp A (2020) Compliant grinding and polishing: A review. *International Journal of Machine Tools and Manufacture* 158:103634.

[285] Zhu W-L, Gao W, Han F, Ju BF, Chen YL, Beaucamp A (2023) Compliant polishing of thin-walled freeform workpiece. *CIRP Annals* 72(1):285–288.

[286] Zhu W-L, Pakenham-Walsh O, Copson K, Charlton P, Tatsumi K, Ju BF, Beaucamp A (2022) Mechanism of mid-spatial-frequency waviness removal by viscoelastic polishing tool. *CIRP Annals* 71(1):269–272.

[287] Zhu W-L, Yang Y, Li HN, Axinte D, Beaucamp A (2019) Theoretical and experimental investigation of material removal mechanism in compliant shape adaptive grinding process. *International Journal of Machine Tools and Manufacture* 142:76–97.

[288] Zhu ZH, Huang P, To S, Zhu LM, Zhu Z (2023) Fast-tool-servo-controlled shear-thickening micropolishing. *International Journal of Machine Tools and Manufacture* 184:103968.

[289] Zmich R, Meyer D (2021) Thermal Effects on Surface and Subsurface Modifications in Laser-Combined Deep Rolling. *Journal of Manufacturing and Materials Processing* 5(2):55.